

## ARTICLE TYPE

## Can high-redshift AGN observed by JWST explain the EDGES absorption signal?

Alexandra Nelander,<sup>1</sup> Christopher Cain,<sup>1</sup> Jordan C. J. D'Silva,<sup>2</sup> Peter H. Sims,<sup>1,3,4</sup> Rogier A. Windhorst,<sup>1</sup> and Judd D. Bowman<sup>1</sup><sup>1</sup>School of Earth and Space exploration, Arizona State University, Tempe, AZ 85281, USA<sup>2</sup>International Centre for Radio Astronomy Research (ICRAR), The University of Western Australia, M468, 35 Stirling Highway, Crawley, WA 6009, Australia<sup>3</sup>Astrophysics Group, Cavendish Laboratory, J. J. Thomson Avenue, Cambridge CB3 0HE, UK<sup>4</sup>Kavli Institute for Cosmology, Madingley Road, Cambridge CB3 0HA, UK

Author for correspondence: Alexandra Nelander, Email: anelande@asu.edu.

## Abstract

The Experiment to Detect the Global Epoch of reionization 21 cm Signal (EDGES) has reported evidence for an absorption feature in the sky-averaged radio background near 78 MHz. A cosmological interpretation of this signal corresponds to absorption of 21 cm photons by neutral hydrogen at  $z \sim 17$ . The large depth of the signal has been shown to require an excess radio background above the CMB and/or non-standard cooling processes in the IGM. Here, we explore the plausibility of a scenario in which the EDGES signal is back-lit by an excess radio background sourced from a population of radio-loud AGN at high redshift. These AGN could also explain the unexpected abundance of UV-bright objects observed at  $z > 10$  by JWST. We find that producing enough radio photons to explain the EDGES depth requires that nearly all high- $z$  UV-bright objects down to  $M_{UV} \gtrsim -15$  are radio-loud AGN and that the UV density of such objects declines by at most 1.5 orders of magnitude between  $z = 10$  and 20. In addition, the fraction of X-ray photons escaping these objects must be  $\lesssim 1\%$  of their expected intrinsic production rate to prevent the absorption signal being washed out by early IGM pre-heating. Re-producing the sharp boundaries of the absorption trough and its flat bottom require that the UV luminosity function, the fraction of UV light produced by AGN, and the X-ray escape fraction have fine-tuned redshift dependence. We conclude that radio-loud AGN are an unlikely (although physically possible) candidate to explain EDGES because of the extreme physical properties required for them to do so.

Keywords: keyword entry 1, keyword entry 2, keyword entry 3

## 1. Introduction

The red-shifted 21 cm signal from neutral hydrogen lies at the frontier of modern cosmology. During and prior to the epoch of reionization (EoR), neutral hydrogen in the intergalactic medium (IGM) absorbed or emitted 21 cm photons via its spin-flip transition, in principle allowing for direct observations of the neutral IGM (Madau, Meiksin, and Rees 1997; Shaver et al. 1999; Gnedin and Shaver 2004; Pritchard and Loeb 2008). Measurements of the sky-averaged signal and its fluctuations have been proposed as probes of reionization (Mesinger and Furlanetto 2007; Datta, Bharadwaj, and Choudhury 2007), the formation and evolution of Pop III stars (Chuzhoy, Alvarez, and Shapiro 2006; Cruz et al. 2024) and black holes (Ripamonti, Mapelli, and Zaroubi 2008), cosmological parameters (McQuinn et al. 2006; Bowman, Morales, and Hewitt 2007), and alternative dark matter models (Valdés et al. 2007; Hibbard et al. 2022), among others. Numerous existing and forthcoming radio experiments are targeting one or more facets of this signal, including EDGES (Bowman et al. 2018), SARAS (Singh et al. 2018), the MWA (Pober et al. 2016), HERA (Berkhout et al. 2024), and the SKA (Koopmans et al. 2015).

The 21 cm signal between the formation of the first stars and the onset of the EoR (at  $10 \lesssim z \lesssim 30$ ) is commonly referred to as the Cosmic Dawn (CD) signal. Early efforts to detect it have targeted the sky-averaged signal, which is expected to be seen in absorption at these redshifts. Recently, the EDGES experiment (Bowman et al. 2018) claimed evi-

dence for the first detection of the CD signal – an absorption trough at  $15 \lesssim z \lesssim 20$  reaching a differential brightness between the 21-cm spin temperature and radio background temperature of  $-500$  mK at  $z = 17$ . The amplitude of the signal is a factor of  $\sim 2 - 3$  larger than the maximum amplitude predicted by concordance CD models (e.g. Meiksin and Madau 2020), and the redshift evolution of the signal is also unusual (Mittal and Kulkarni 2022). Indeed, several works have questioned its cosmological origin. Notably, the SARAS 3 experiment claimed a non-detection of the signal amplitude claimed by EDGES at 95% confidence (Singh et al. (2022), see also Bevins et al. (2022)). Concerns have also been raised over the techniques used to model the sky-averaged radio signal used by EDGES (e.g. Hills et al. 2018; Sims and Pober 2020; Cang et al. 2024). However, the possibility that the signal is of cosmological origin remains open and of interest.

Several mechanisms have been proposed to explain the non-standard depth of the EDGES feature. These generally involve either non-standard cooling of the neutral IGM, perhaps due to interactions with dark matter (e.g. Datta et al. 2020; Halder and Banerjee 2021), or a radio background in excess of the CMB (Natwariya (e.g. 2021) and Mittal et al. (2022), although see Cang et al. (2024)). In the latter scenario, which will be the focus of this work, several mechanisms have been proposed to produce the required excess radio emission. These include accreting black holes (Ewall-Wice et al. 2018; Ewall-Wice, Chang, and Lazio 2020), an excess of faint galaxies at high red-

shifts (Mirocha and Furlanetto 2019), or unexpected sources of galactic radio emission (Reis, Fialkov, and Barkana 2020). The detection of an excess low-frequency radio background by ARCADE-2 (Fixsen *et al.* 2011) at low redshift lends plausibility to this explanation (see also Tompkins *et al.* (2023)).

JWST observations are closing in on the redshift range probed by EDGES. The latest constraints on the UV luminosity function (UVLF) of galaxies have pushed as high as  $z = 14$  (Adams *et al.* 2023; C T Donnan *et al.* 2024; Finkelstein *et al.* 2024a)<sup>a</sup>. One key finding is an unexpectedly high abundance of bright galaxies at  $z > 10$ , which have strained pre-JWST models of galaxy formation (Chemerynska *et al.* 2024; Lu *et al.* 2025; Harikane *et al.* 2025; Whitler *et al.* 2025), and perhaps even  $\Lambda$ CDM cosmology itself (Boylan-Kolchin 2023). Explanations for this excess include increased star formation efficiency at high redshift (Jeong *et al.* 2025), younger stellar populations (C. T. Donnan *et al.* 2025), excess light from accreting black holes (Matter, Pallottini, and Ferrara 2025), and more exotic scenarios such as early dark energy (Shen *et al.* 2024).

A compelling possibility is that a large population of radio-loud accreting black holes at  $10 \lesssim z \lesssim 20$  explains both of these puzzles. There is some observational support for the possibility that a significant fraction of the  $z > 10$  UV light seen by JWST is produced by AGN. Recently, D’Silva *et al.* (2023) fit the SEDs of bright galaxies at  $z \sim 10.5$  and found that around half of the UV light could be explained by an AGN contribution (see also D’Silva *et al.* (2025)). Along the same lines, Hegde, Wyatt, and Furlanetto (2024) found that up to half the light produced by  $z > 10$  objects could plausibly come from AGN without violating constraints on galaxy morphology (Ono *et al.* 2023). If a large fraction of these objects are radio-loud AGN that begin growing at  $z > 15$ , they may also produce enough radio emission at these redshifts to back-light EDGES in combination with the CMB (Ewall-Wice *et al.* 2018; Ewall-Wice, Chang, and Lazio 2020).

This scenario finds additional motivation from observations of bright quasars at lower redshifts. An increasingly large sample of bright AGN have been detected within the first billion years of cosmic history ( $z \gtrsim 6$ ), with masses often inferred to be  $10^9 M_\odot$  or more (Wu *et al.* 2015; Eduardo Bañados *et al.* 2018; Eilers, Davies, and Hennawi 2018; J. Yang *et al.* 2020; Bennett *et al.* 2024). Indeed, such black holes are often observed to be over-massive relative to their host galaxies, suggesting a possible early onset of AGN growth relative to stellar formation (Sun *et al.* 2025). Growing such massive black holes by these redshifts generally requires massive seeds (Woods *et al.* 2019), super-Eddington accretion (Johnson and Upton Sanderbeck 2022) and/or low radiative efficiencies (Morey *et al.* 2021). In any case, it is reasonable to expect that rapidly growing AGN should exist at much higher redshifts.

In this work, we investigate the possibility that a large population of  $z > 10$  AGN could explain JWST observations and the EDGES signal. We use observations of the UVLF

up to  $z = 14$  from JWST, extrapolated to higher redshifts, to model the excess radio background produced by AGN. We also account for the effect AGN would have on Ly $\alpha$  coupling of the 21 cm spin temperature to the IGM gas temperature and the pre-heating of the IGM by X-rays. This work is organized as follows. In §2, we describe our formalism for modeling the sky-averaged 21 cm signal. §3 presents our main results, and in §4 we discuss implications of our findings for interpreting high-redshift observations. We conclude in §5. Throughout, we assume the following cosmological parameters:  $\Omega_m = 0.305$ ,  $\Omega_\Lambda = 1 - \Omega_m$ ,  $\Omega_b = 0.048$ ,  $h = 0.68$ ,  $n_s = 0.9667$  and  $\sigma_8 = 0.82$ , consistent with Planck Collaboration *et al.* (2020) results. Distances are in co-moving units unless otherwise specified.

## 2. Modeling the cosmic dawn global 21 cm signal

### 2.1 Basics of the signal

The sky-averaged 21 cm absorption temperature during the CD and reionization is given by

$$T_{21}(z) = \bar{T}_{21}^0 (1+z)^{\frac{1}{2}} x_{\text{HI}}(z) \left[ 1 - \frac{T_{\text{radio}}(z)}{T_S(z)} \right] \quad (1)$$

where  $\bar{T}_{21}^0 = 8.5 \left( \frac{\Omega_b}{0.044} \right) \left( \frac{h}{0.7} \right) \left( \frac{\Omega_m}{0.27} \right)^{\frac{1}{2}}$  mK is independent of redshift (Giri *et al.* 2019),  $x_{\text{HI}}(z)$  is the mass-averaged IGM neutral fraction,  $T_{\text{radio}}$  is the radio background temperature at 1.4GHz and  $T_S$  is the spin temperature of neutral IGM gas. During the CD,  $x_{\text{HI}} = 1$ , and the redshift evolution of the signal is driven by that of  $T_{\text{radio}}$  and  $T_S$ . In standard scenarios, the radio background is taken to be that of the CMB – namely,  $T_{\text{radio}} = T_{\text{CMB}} = 2.7(1+z)$  K. In cases with an external radio background  $T_{\text{ex}}$ , we write  $T_{\text{radio}} = T_{\text{CMB}} + T_{\text{ex}}$ . Note that  $T_{\text{ex}} > 0$  is required, in canonical 21 cm models, to achieve  $T_{21}$  much less than  $-200$  mK by  $z = 17$  (see e.g. Figure 2 of Cang *et al.* (2024)).

When the first stars form, the Lyman-Werner (LW) radiation they produce couples  $T_S$  to the gas kinetic temperature. Ignoring collisional coupling (which is unimportant at  $z < 30$ ), the coupling is described by

$$T_S^{-1} = \frac{T_{\text{radio}}^{-1} + x_\alpha T_K^{-1}}{1 + x_\alpha} \quad (2)$$

where  $x_\alpha$  is the Ly $\alpha$  coupling coefficient. In canonical 21 cm models (e.g. Furlanetto (2006)), coupling is started by pop III stars, since these are the first sources of UV radiation. Prior to pre-heating by the first X-ray sources, the IGM has kinetic temperature  $T_K < T_{\text{CMB}}$ , such that the average signal is negative (appears in absorption, Eq. 1). Heating of the neutral IGM by X-rays before reionization (“pre-heating”) likely raises  $T_K$  well above  $T_{\text{CMB}}$  by  $z \sim 10$ , such that the EoR signal appears in emission. Later in this section, we will describe how we model the key components driving the CD signal – the excess radio background  $T_{\text{ex}}$  (§2.3), Ly $\alpha$  coupling (§2.4), and X-Ray heating (§2.5).

a. See Pérez-González *et al.* (2025) and Castellano *et al.* (2025) for tentative constraints at higher redshifts.

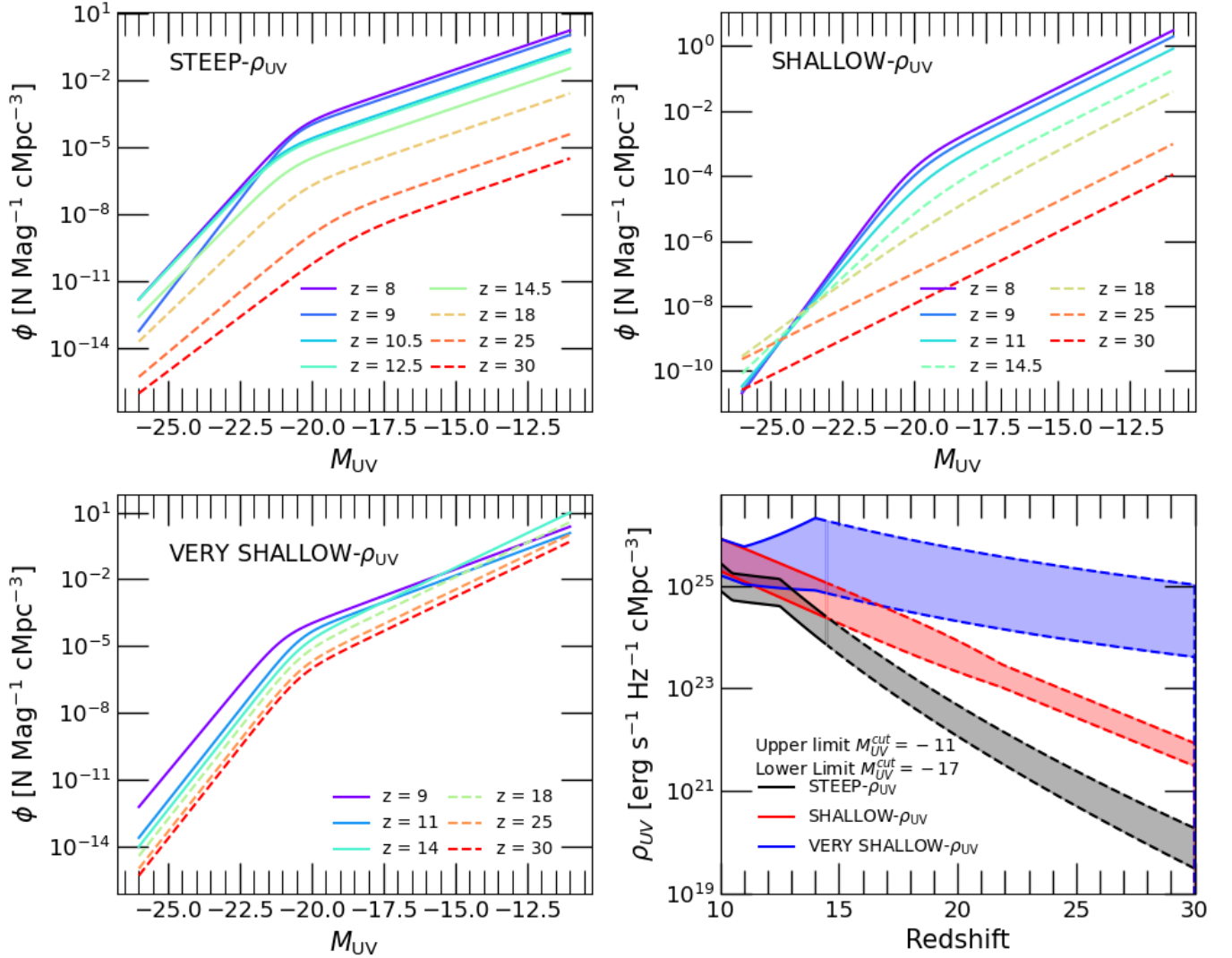


**Figure 1.** UVLFs assumed in this work and their associated UV luminosity densities. **Top Left:** UVLFs for the STEEP- $\rho_{\text{UV}}$  model, which uses measurements from Adams et al. (2023) at  $8 \leq z \leq 12.5$  and C T Donnan et al. (2024) at  $z = 14.5$ . Solid curves denote redshifts where measurements are available, and dashed curves are extrapolations up to  $z = 30$ . **Top Right:** the same for our SHALLOW- $\rho_{\text{UV}}$  model, which extrapolates the redshift-dependent fits to the UVLF parameters in Eq. 3-6 of C T Donnan et al. (2024). **Bottom Left:** our VERY SHALLOW- $\rho_{\text{UV}}$  model, based on extrapolating the UVLF measurements at  $z = 9, 11$ , and 14 from Finkelstein et al. (2024a). **Bottom Right:** the UV luminosity density,  $\rho_{\text{UV}}$ , for all three models. The shaded range denotes the difference between assuming bright ( $M_{\text{UV}} < -17$ ) and faint ( $M_{\text{UV}} < -11$ ) integration limits. Dashed lines denote extrapolations from measurements.

## 2.2 JWST UV Luminosity Functions

In this work, we base our model for the CD 21 cm signal on measurements of the UV luminosity functions (UVLF) by JWST up to  $z \approx 14$  (e.g. Adams et al. 2023; Finkelstein et al. 2024a; C T Donnan et al. 2024). Our premise is that a significant fraction of UV-luminous objects during the CD are radio-loud AGN. In Figure 1, we show three models for the UVLF considered in this work, which are based on recent JWST observations at  $10 < z < 14$ . The top left, top right, and bottom left panels show the UVLF for each model, with solid curves denoting redshifts where measurements are available and dashed lines denoting extrapolations to higher redshifts (discussed below). In the bottom right, we show the UV luminosity density,  $\rho_{\text{UV}}$ , for each model, with dashed lines indicating extrapolations. The shaded region shows the range

obtained from integrating each set of UVLFs down to limiting magnitudes of  $M_{\text{UV}} = -17$  and  $-11$ .

The top left panel shows our STEEP- $\rho_{\text{UV}}$  model, which uses measurements at  $8 \leq z \leq 12.5$  from Adams et al. (2023) and the C T Donnan et al. (2024) measurement at  $z = 14.5$ . These fits (and all the others we use) assume a double power-law for the UVLF of the form

$$\frac{dn}{dM_{\text{UV}}} = \frac{\phi^* \ln 10}{2.5} \left( \left[ 10^{0.4(M_{\text{UV}} - M_*)} \right]^{\alpha+1} + \left[ 10^{0.4(M_{\text{UV}} - M_*)} \right]^{\beta+1} \right)$$

where  $\alpha$  is the faint-end slope,  $\beta$  is the bright end slope,  $M_*$  is the cutoff between bright and faint ends, and  $\phi^*$  is the amplitude parameter. We linearly extrapolate the shape parameters in redshift -  $\alpha$ ,  $\beta$ , and  $M_*$  - between the  $z = 12.5$  and  $14.5$  measurements, and do a log-linear extrapolation of  $\phi^*$ . This

UVLF model falls off rapidly with redshift, with  $\rho_{\text{UV}}$  dropping 4 orders of magnitude between  $z = 14$  and 30 (bottom right). The top right panel shows our SHALLOW- $\rho_{\text{UV}}$  model, which uses Eq. 3–6 for the UVLF parameters in C T Donnan et al. (2024) to predict the UVLF out to  $z = 30$ . These equations were calibrated to best match a collection of measurements at  $8 < z < 14$  from (R. A. A. Bowler et al. 2016; R A A Bowler et al. 2020; C T Donnan et al. 2022; McLeod et al. 2023). They predict that the bright-end slope,  $\beta$ , should increase rapidly with redshift, becoming larger than the faint-end slope,  $\alpha$ , at  $z \sim 25$ . To avoid un-physical behavior in the UVLF,<sup>b</sup> we impose the condition that  $\beta \leq \alpha$  at all redshifts.

The bottom left panel shows our VERY SHALLOW- $\rho_{\text{UV}}$  model, which is based on recent measurements at  $z = 9, 11$ , and 14 by Finkelstein et al. (2024a). They find that  $\rho_{\text{UV}}$  integrated down to  $M_{\text{UV}} = -17$  is nearly flat (evolves only a factor of a few) between redshifts 9 and 14. They further find a relatively steep faint-end slope of  $\alpha = -2.55$  at  $z = 14$ , which predicts an increase in  $\rho_{\text{UV}}$  with redshift when integrated to  $M_{\text{UV}} = -11$  (see lower right panel). Extrapolating their measurements to  $z = 30$  (assuming  $\alpha = -2.55$  at  $z > 14$ ) predicts only one order of magnitude decrease in  $\rho_{\text{UV}}$  across this redshift range. For this model, we must impose the additional condition that  $\phi^*(z > 30) = 0$  to avoid un-physically high UV light production extending into the cosmic dark ages (before there was sufficient structure formation to produce halos capable of hosting galaxies).

Estimating the radio and X-ray emissions of an AGN from its UV luminosity  $L_{\text{UV}}$  requires an estimate of its black hole mass,  $M_{\text{bh}}$ . The associated bolometric luminosity is given by (Hegde, Wyatt, and Furlanetto 2024)

$$L_{\text{bh}} = 3.3 \times 10^4 \times \eta_{\text{edd}} M_{\text{bh}} \quad (3)$$

where  $\eta_{\text{edd}}$  is the Eddington ratio. Following Hegde, Wyatt, and Furlanetto (2024), we map bolometric luminosity to UV luminosity using the procedure described in Marconi et al. (2004), which yields

$$L_{\text{UV}} = \frac{L_{\text{bh}}}{\nu_b^{10^{0.8-0.067\gamma+0.017\gamma^2-0.0023\gamma^3}}} \times \left( \frac{\nu_{\text{UV}}}{\nu_b} \right)^{-\alpha_{\text{UV}}} \quad (4)$$

where  $\nu_b = 6.67 \times 10^{14}$  Hz and  $\nu_{\text{UV}} = 2 \times 10^{15}$  Hz and  $\gamma = \log_{10}(L_{\text{bh}}/L_{\odot}) - 12$ . We assume a UV slope of  $\alpha_{\text{UV}} = 0.6$ , typical for bright quasars at lower redshifts (Lusso et al. 2015). Assuming a given object's UV emission is dominated by the AGN, Eq. 3–4 can be used to map between  $L_{\text{UV}}$  and  $M_{\text{bh}}$ . We have tested how much our results vary across the range  $0.45 < \alpha_{\text{UV}} < 0.7$  (Vanden Berk et al. 2001; Telfer et al. 2002) and found a difference in  $T_{21}$  of  $\approx 35\%$  across this range. Though non-negligible, this effect is sub-dominant relative to other sources of uncertainty in our analysis.

b. The symmetric form of the double power law function used to fit the UVLF implies that  $\max(\alpha, \beta)$  behaves as the faint-end slope. Thus, allowing  $\beta > \alpha$  swaps the function of the two variables. Our condition avoids this behavior.

### 2.3 Excess radio background from AGN

The total radio emissivity of the AGN population at redshift  $z$  and frequency  $\nu$  can be written as

$$\epsilon(\nu, z) = f_l f_{\text{bh}} \int_{-\infty}^{M_{\text{UV}}^{\text{cut}}} dM_{\text{UV}} \frac{dn}{dM_{\text{UV}}} L_{\nu, \text{radio}}(M_{\text{UV}}) \quad (5)$$

where  $f_l$  is the fraction of AGN that are radio-loud,  $M_{\text{UV}}^{\text{cut}}$  is the cutoff between objects dominated by AGN and stellar light,  $f_{\text{bh}}$  is the fraction of objects with  $M_{\text{UV}} < M_{\text{UV}}^{\text{cut}}$  that are AGN,  $dn/dM_{\text{UV}}$  is the UVLF, and  $L_{\nu, \text{radio}}(M_{\text{UV}})$  is the radio luminosity of an AGN with magnitude  $M_{\text{UV}}$ . Note that  $M_{\text{UV}}^{\text{cut}}$  is defined here as the cutoff in the UVLF between AGN and stellar-driven UV sources, *not the faint-end turnover of the UVLF*. We estimate the radio luminosity at 5GHz,  $L_{5\text{GHz}}$ , using recent measurements of the fundamental plane of radio-loud quasars from Bariuan et al. (2022),

$$\log_{10}[L_{5\text{GHz}}/\text{erg s}^{-1}] = b + \xi_x \log_{10}[L_{2-10}/\text{erg s}^{-1}] + \xi_m \log_{10}[M_{\text{bh}}/M_{\odot}] \quad (6)$$

where  $\xi_x = 1.12$ ,  $\xi_m = -0.210$ , and  $b = -5.64$  and  $L_{2-10}$  is the intrinsic X-ray luminosity of the AGN between 2 and 10 keV. This is given by

$$L_{2-10} = k_{\text{bol}}^{-1} \eta_{\text{edd}} L_E \quad (7)$$

where  $k_{\text{bol}}^{-1} = 0.07$  is the bolometric correction factor (Lusso et al. 2010) and  $L_E = 1.26 \times 10^{38} \text{ erg s}^{-1} \frac{M_{\text{bh}}}{M_{\odot}}$  is the Eddington luminosity. The radio luminosity per unit frequency  $L_{\nu, \text{radio}}$  is then given by

$$L_{\nu, \text{rad}} = \frac{L_{5\text{GHz}}}{5\text{GHz}} \left( \frac{\nu}{5\text{GHz}} \right)^{-\alpha_{\text{radio}}} \quad (8)$$

where we take  $\alpha_{\text{radio}} = 0.5$  following the assumed scaling<sup>c</sup> in Bariuan et al. (2022). The corresponding radio temperature at 1.4 GHz ( $T_{\text{ex}}$  in §2.1) is given in terms of  $\epsilon(\nu, z)$  by Eq. 5–6 of Ewall-Wice et al. (2018). The fundamental plane relation in Bariuan et al. (2022) reports a logarithmic scatter of  $\sigma_R \approx 0.5$  (in a fixed redshift bin). Assuming that the underlying distribution is lognormal around the best-fit relation, this corresponds to a factor of  $\approx 2$  boost for the average radio emission relative to the best-fit relation in log space. We multiply the  $L_{5\text{GHz}}$  given by Eq. 6 by a factor of 2 to correct for intrinsic scatter.

There is considerable uncertainty in the radio-loud fundamental plane given by Eq. 6. Figure 4 of Bariuan et al. (2022) shows that there is nearly an order of magnitude of scatter on either side of their best-fit relation, and they noted potential redshift evolution. Furthermore, Wang et al. (2024) found somewhat lower radio emission than in Bariuan et al. (2022),

c. Measurements used in Bariuan et al. (2022) are made close to 1.4GHz and extrapolated to 5GHz assuming  $\alpha_{\text{radio}} = 0.5$ , so this re-scaling recovers the exact measured flux at 1.4GHz. Physically, there is significant scatter in  $\alpha_{\text{radio}}$  for quasars of different types (Gloude-mans et al. 2022) – however, our results are sensitive only to radio emission at frequencies close to 1.4GHz, and thus modest differences in  $\alpha_{\text{radio}}$  have a minimal effect on our results.

and commented on possible extra dependencies not considered in that work (see also Long et al. (2025)). There is also variation (a dex or more) in the hard X-ray bolometric correction factors observed for AGN. Our choice of  $k_{\text{bol}} = 0.07^{-1} = 14.3$  is on the low end of the distribution observed in Lusso et al. (2010) and Lusso et al. (2012), and in more recent work by Spinoglio, Fernández-Ontiveros, and Malkan (2024). It is also consistent with the values predicted for low-luminosity AGN by Duras et al. (2020). Higher  $k_{\text{bol}}$  would result in lower  $L_{2-10}$  at fixed  $M_{\text{bh}}$ , and thus reduced  $L_{5\text{GHz}}$ , which would in turn produce a weaker radio background. As we will see in later sections, assuming a relatively low  $k_{\text{bol}}$  is conservative for the purposes of this work.

## 2.4 Ly $\alpha$ coupling

UV photons with energies between 11.2 and 13.6 eV (Lyman-Werner photons) from the first stars/AGN coupled the spin temperature of the 21 cm transition to the kinetic temperature of the neutral gas, a process known as Ly $\alpha$  coupling. This occurs by means of the Wouthuysen-field effect via transitions to the 2p state of neutral hydrogen (Wouthuysen 1952; Field 1958; Hirata 2006). We describe in this section how we model the contribution to Ly $\alpha$  coupling from pop II stars/AGN and pop III stars.

### 2.4.1 Pop II stars & AGN

The Ly $\alpha$  coupling coefficient,  $x_{\alpha}$  (see Eq. 2) is given by

$$x_{\alpha} = \frac{4\pi e^2 f_{\alpha} T^*}{27 A_{10} T_{\text{CMB}} m_e} S_{\alpha} n_{\alpha} \quad (9)$$

where  $T^* = 68.2$  mK,  $f_{\alpha} = 0.4162$ ,  $A_{10} = 2.87 \times 10^{-15} \text{ s}^{-1}$ ,  $e$  is the electron charge,  $T_{\text{CMB}}$  is the CMB temperature and  $m_e$  is the electron mass. The scattering correction,  $S_{\alpha}$ , is given by

$$S_{\alpha} = \exp\left(-0.013 \tau_{\text{GP}}^{1/3} / T_{\text{K}}^{2/3}\right) \quad (10)$$

where  $\tau_{\text{GP}}$  is the Gunn-Petersen optical depth and  $T_{\text{K}}$  is the gas kinetic temperature. The number density of Ly $\alpha$  photons is given by (Madau 2018),

$$n_{\alpha}(z) = (1+z)^2 \sum_{n=2}^{\infty} P_{np} \int_z^{z_{\text{max}}(n)} \dot{n}_{\nu'}(z') \frac{dz'}{H(z')} \quad (11)$$

where the sum runs over the transitions from  $n$ th excited state of Ly $\alpha$  to the ground state. Here,  $\nu' = \nu_n(1+z')/(1+z)$ , where  $\nu_n$  is the frequency of the  $n$ th excited state. For the  $n$ th excited state, the upper limit of the integral is

$$z_{\text{max}}(n) = (1+z) \frac{1 - \frac{1}{n^2}}{1 - \frac{1}{(n+1)^2}} \quad (12)$$

The number density of UV photons produced by pop II stars and AGN is given in terms of the UV luminosity density as

$$\dot{n}_{\nu}(z) = \left( \frac{\rho_{\text{UV}}(z)}{h_{\text{p}} \nu_{\text{UV}}} \right) \left( \frac{\nu}{\nu_{\text{UV}}} \right)^{-\alpha_{\text{UV}}-1} \quad (13)$$

where again we have taken  $\alpha_{\text{UV}} = 0.6$ . We assume here that the faint-end turnover happens at  $M_{\text{UV}} = -11$ , such that we integrate down to that limit to get  $\rho_{\text{UV}}$  in Eq. 13. In our model, the UVLF at  $M_{\text{UV}} < M_{\text{UV}}^{\text{cut}}$  is dominated by AGN, and fainter objects are dominated by pop II stars.

### 2.4.2 Pop III Stars

Pop III stars were probably the first drivers of Ly $\alpha$  coupling. These first stars likely formed predominantly in halos well below the atomic cooling limit (masses  $< 10^8 M_{\odot}$ ), the so-called “mini-halos” (Miralda-Escudé 2003). As such, these stars likely formed in halos much below the visibility limits of current observations (Windhorst et al. 2018), and/or may not contribute significantly to the total star formation rate at  $z < 15$  (Visbal, Bryan, and Haiman 2020). As such, that they would likely not be accounted for in our extrapolations of the UVLF in Figure 1 (although see Fujimoto et al. (e.g. 2025) and Venditti et al. (2025) for suggestions that some Pop III stars may live in more massive halos). We include the contribution of Pop III stars to Ly $\alpha$  coupling using the analytic prescription described in McQuinn and O’Leary (2012). The star formation rate density of pop III stars is given by

$$\rho_{\text{SFR}}^{\text{III}} = f_* \rho_b \frac{d}{dt} \left[ \rho_m^{-1} \int_{M_{\text{crit}}}^{M_{\text{atom}}} dM \left( \frac{dn}{dM} \right) M \right] \quad (14)$$

where  $f_*$  is the pop III star formation efficiency,  $\rho_b$  and  $\rho_m$  are the baryon and total matter densities, and  $dn/dM$  is the Sheth-Tormen halo mass function (Sheth and Tormen 1999). The expression in brackets is the fraction of mass collapsed in molecular cooling halos hosting pop III star formation. The upper limit of the integral is the atomic cooling limit, which we take to be  $M_{\text{atom}} = 10^8 M_{\odot}$ , and the lower limit is the critical mass for molecular hydrogen formation (Machacek, Bryan, and Abel 2001),

$$M_{\text{crit}} = 2.5 \times 10^5 + 8.7 \times 10^5 F_{\text{LW},21}^{0.47} M_{\odot} \quad (15)$$

where the normalized Lyman-Werner intensity is

$$F_{\text{LW},21} = 20 \left( \frac{1+z}{21} \right) e^{-\tau_{\text{LW}}} \text{erg s}^{-1} \quad (16)$$

and we take  $\tau_{\text{LW}} = 1.5$ . We can approximate the coupling coefficient due to UV emission from pop III star by inverting Eq. 7 of McQuinn and O’Leary (2012), which yields

$$x_{\alpha}^{\text{III}} = \frac{\rho_{\text{SFR}}^{\text{III}}}{1.7 \times 10^{-3} M_{\odot} \text{yr}^{-1} \text{cMpc}^{-3}} \frac{N_{\alpha}}{10^4} \left( \frac{1+z}{21} \right) \quad (17)$$

and the total coupling coefficient is given by linearly adding this term to the pop II/AGN component given by Eq. 9.

In Figure 2, we show the evolution of  $x_{\alpha}$  with redshift in our SHALLOW- $\rho_{\text{UV}}$  (top) and VERY SHALLOW- $\rho_{\text{UV}}$  (bottom) models. In each panel, the solid black curve shows the total  $x_{\alpha}$ , while the dot-dashed red and dashed blue curves show the contribution from pop III stars and pop II stars/AGN, respectively. The vertical dashed line denotes  $z = 17$ , the central

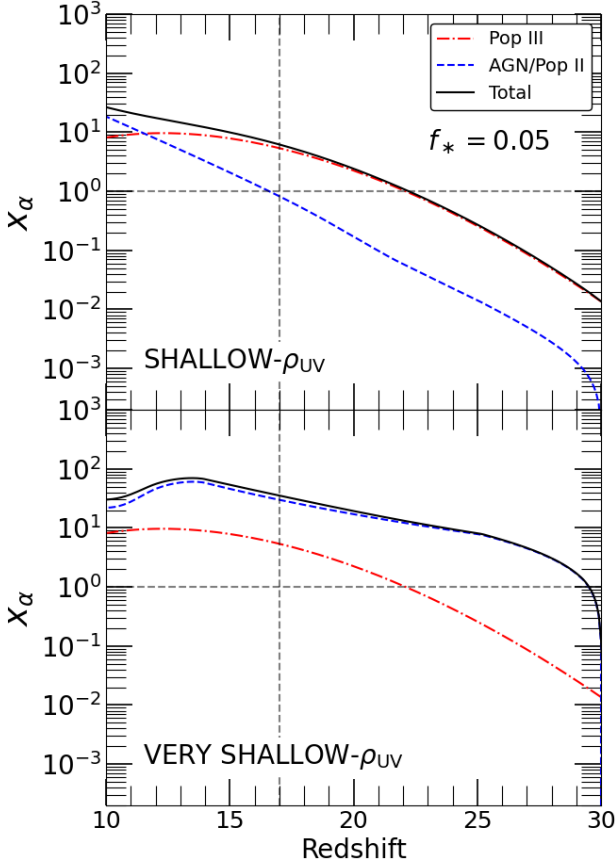


**Figure 2.** Ly $\alpha$  coupling coefficient in our SHALLOW- $\rho_{UV}$  (top) and VERY SHALLOW- $\rho_{UV}$  (bottom) models. The solid black line denotes the total  $x_\alpha$ , and the dot-dashed red and dashed blue lines the contributions from pop III stars and pop II star/AGN, respectively. The vertical dashed line denotes  $z = 17$ , the central EDGES redshift, and the horizontal line  $x_\alpha = 1$ , at which coupling is halfway complete. We choose  $f_* = 0.05$  for pop III stars, such that coupling is well underway by  $z = 20$ , as required by the EDGES signal. In the SHALLOW- $\rho_{UV}$  case, coupling is dominated by pop III stars, but in the VERY SHALLOW- $\rho_{UV}$  case it is dominated by the pop II/AGN component.

redshift of the EDGES signal, and the horizontal line indicates  $x_\alpha = 1$ , for which coupling is halfway complete. We chose  $f_* = 0.05$  (within the range assumed in McQuinn and O’Leary (2012)) so that coupling is well underway by  $z = 20$ , as required by the EDGES signal. In the STEEP- $\rho_{UV}$  (not shown) and SHALLOW- $\rho_{UV}$ , pop III stars dominate Ly $\alpha$  coupling at  $z > 15$  for this value of  $f_*$ . However, in the VERY SHALLOW- $\rho_{UV}$  model, coupling occurs abruptly at  $z = 30$  and is dominated by the pop II/AGN component<sup>d</sup>.

We note that a number of works more recent than McQuinn and O’Leary (2012) have provided updated estimates of  $M_{\text{crit}}$  (Equation 15), which take into account more accurately the effects of Lyman Werner suppression and baryon-dark matter streaming velocities (e.g. Kulkarni, Visbal, and Bryan 2021; Nebrin, Giri, and Mellema 2023; Hegde and Furlanetto

d. Indeed, coupling in this model would begin much earlier than  $z = 30$  without our condition that  $\Phi^*(z > 30) = 0$ .

2023). These works, in general, find somewhat lower  $M_{\text{crit}}$  than we assume here, which would result in earlier, faster Ly $\alpha$  coupling. However,  $M_{\text{crit}}$  is mostly degenerate with  $f_*$ , which we tuned to produce coupling within a redshift range favorable for EDGES. As such, using these improved estimates of  $M_{\text{crit}}$  would have little impact on our results in this work.

## 2.5 X-Ray heating

X-ray photons have ionizing cross-sections small enough to allow them to travel cosmological distances through the neutral IGM. The first X-ray sources are believed to have pre-heated the IGM to  $T_K > T_{\text{CMB}}$  before the onset of reionization (Fialkov, Barkana, and Visbal 2014; HERA Collaboration *et al.* 2023). This resulted in  $T_{\text{radio}}/T_S \rightarrow 0$  in Eq. 1, driving the signal out of absorption and into emission. The steep rise of the EDGES absorption signal towards 0 at  $z \approx 15$  is most naturally interpreted as the result of X-ray heating.

Absent non-standard heating or cooling channels, the temperature of the neutral IGM before reionization is given by

$$\frac{dT}{dt} = -2H(z)T + \frac{2}{3n_{\text{tot}}k_b}H_{\text{X-ray}} \quad (18)$$

where  $H_{\text{X-ray}}$  is the heating rate from X-rays,  $n_{\text{tot}}$  is the particle number density of the IGM, and the other symbols have their usual meanings. In this work, we assume that all X-ray heating is sourced by AGN, which gives a conservative estimate of the heating rate. In reality, additional contributions are expected from pop III stars (Xu *et al.* 2016) and/or pop II high-mass X-ray binaries (HMXBs, Fialkov, Barkana, and Visbal 2014; Madau and Fragos 2017).

The X-ray luminosity at frequency  $\nu$  by an AGN with magnitude  $M_{UV}$  is given by

$$L_x(\nu, M_{UV}) = \left(\frac{\nu}{\nu_2}\right)^{-\alpha_X} \frac{(1 - \alpha_X)L_{2-10}(M_{UV})}{\nu_2 [5^{(1-\alpha_X)} - 1]} \quad (19)$$

where  $\nu_2 \equiv 2 \text{ keV}/h_p$  and the factor of 5 is the ratio of 10 keV and 2 keV,  $L_{2-10}$  is given by Eq. 7, and  $\alpha_X$  is the slope of the X-ray spectrum of AGN. Following Ewall-Wice *et al.* (2018), we assume  $\alpha_X = 0.9$ . We have denoted in Eq. 19 that  $L_{2-10}$  is a function of  $M_{UV}$  (Eq. 3-4). The co-moving emissivity of X-ray photons at frequency  $\nu$  and redshift  $z$  is given by

$$\dot{N}_X(z, \nu) = f_{\text{esc}}^X \frac{1}{h_p \nu} \int_{-\infty}^{M_{UV}^{\text{cut}}} dM_{UV} \frac{dn}{dM_{UV}} L_X(M_{UV}, \nu) \quad (20)$$

where  $f_{\text{esc}}^X$  is the escape fraction of X-ray photons, which we assume (for simplicity) is independent of photon energy. The number density of X-Ray photons in the universe at frequency  $\nu$  and redshift  $z$  is given by

$$N_X(\nu, z) = \int_{-\infty}^z dz' \left| \frac{dt'}{dz'} \right| \dot{N}_X(z', \nu') \exp[-\tau'(\nu', z', \nu, z)] \quad (21)$$



where  $\nu' = (1+z')/(1+z)\nu$  and  $\tau'$  is the optical depth encountered by X-rays emitted at  $z'$  with frequency  $\nu'$  by the time they redshift to frequency  $\nu$  at redshift  $z$ . We can approximate this by

$$\tau'(\nu', z', \nu, z) \approx \kappa(\nu, z)c(t-t') \quad (22)$$

where  $t$  and  $t'$  are the cosmic times at redshifts  $z$  and  $z'$  (respectively), and  $\kappa(z, \nu)$  is the absorption coefficient of the IGM to X-rays, given by

$$\kappa(z, \nu) = \sigma_{\text{HI}}(\nu)n_{\text{H}}(z) + \sigma_{\text{HeI}}(\nu)n_{\text{He}}(z) \quad (23)$$

where  $\sigma$  and  $n$  are the absorption cross-sections and number densities for HI and HeI in a neutral IGM. Note that Eq. 22 neglects the dependence of  $\kappa$  on  $z'$  and  $\nu'$  along the line of sight. Fortunately, this approximation is reasonable thanks to the frequency dependence of the cross-sections of HI and HeI<sup>e</sup>. The heating rate is then given by

$$H_{\text{X-ray}}(z) = n_{\text{H}}(z)(1+z)^3 \int_{\nu_{0.5}}^{\nu_{10}} N_{\text{X}} \epsilon \sigma_{\text{HI}}(\nu) (h_{\text{p}} \nu) d\nu \quad (24)$$

where we have neglected the sub-dominate contribution to the heating rate from ionizations of He. We have integrated down to 0.5 keV to include heating from soft X-rays.

We note here that our analysis neglects the effects of heating from Ly $\alpha$  photons and the CMB. Reis, Fialkov, and Barkana 2021 found that, in cases where heating from other sources (such as X-rays, see below) is very low, it can have a significant effect on the maximum depth of the 21 cm absorption feature. As we will see in the next section, the signal is hard to reproduce with radio emission from AGN even under optimistic circumstances. Since our goal here is to understand the minimal requirements for our model to achieve the EDGES depth at  $15 < z < 20$ , neglecting this effect is a conservative assumption with respect to our main results. At  $z < 15$ , Reis, Fialkov, and Barkana 2021 found that this heating source negligibly affects  $T_{21}$  if the gas temperature is  $\gtrsim 100$  K by  $z = 10$ , which it is in all the models we consider below that include heating effects. As such, we expect that our results would be qualitatively unaffected by the inclusion of Ly $\alpha$  and CMB heating.

In Figure 3, we show the evolution of the gas temperature predicted by our AGN heating model for several scenarios. The black solid curve is “adiabatic limit”, without any pre-heating, and the dashed black curve shows  $T_{\text{CMB}}$ . The red dotted, solid, and dashed curves show  $T_{\text{K}}$  vs.  $z$  for our SHALLOW- $\rho_{\text{UV}}$  model assuming several combinations of  $f_{\text{esc}}^{\text{X}}$  and  $M_{\text{UV}}^{\text{cut}}$ , indicated in the legend, in order of increasing heating rate. The solid magenta and blue curves show  $T_{\text{K}}$  for  $f_{\text{esc}}^{\text{X}} = 1$  and  $M_{\text{UV}}^{\text{cut}} = -17$  for the STEEP- $\rho_{\text{UV}}$  and VERY SHALLOW- $\rho_{\text{UV}}$  models, respectively. The vertical dotted line denotes  $z = 17$ .

Models with higher UV densities, fainter  $M_{\text{UV}}^{\text{cut}}$ , and higher  $f_{\text{esc}}^{\text{X}}$  produce larger IGM temperatures. All these scenarios begin pre-heating the IGM at  $z > 17$ , and some of them have

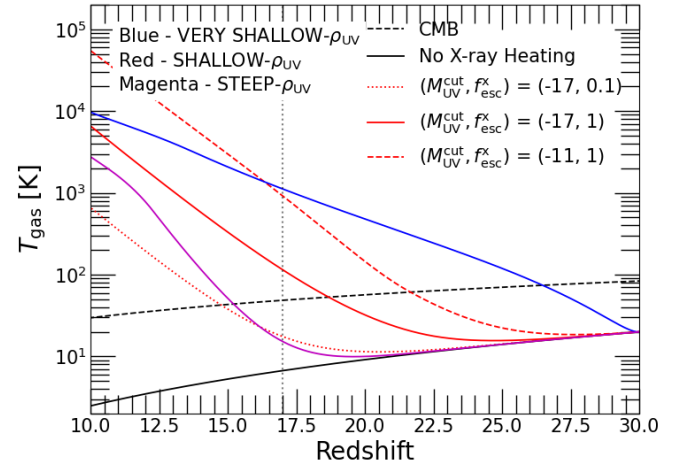


**Figure 3.** Examples of thermal histories predicted by our AGN-driven pre-heating model for several representative scenarios. The solid and dashed black curves show the temperature absent pre-heating (the adiabatic limit) and the CMB temperature, respectively. For the SHALLOW- $\rho_{\text{UV}}$  model, we show  $T_{\text{K}}$  for  $(f_{\text{esc}}^{\text{X}}, M_{\text{UV}}^{\text{cut}}) = (0.1, -17)$ ,  $(1, -17)$ , and  $(1, -11)$  as the red dotted, solid, and dashed curves, respectively. We also show the STEEP- $\rho_{\text{UV}}$  and VERY SHALLOW- $\rho_{\text{UV}}$  models assuming  $(f_{\text{esc}}^{\text{X}}, M_{\text{UV}}^{\text{cut}}) = (1, -17)$  as the magenta and blue solid curves. Models with higher  $f_{\text{esc}}^{\text{X}}$ , fainter  $M_{\text{UV}}^{\text{cut}}$ , and higher UV densities predict earlier pre-heating and higher temperatures.

already reached gas temperatures above  $T_{\text{CMB}}$  by this redshift. This indicates that X-ray pre-heating by AGN can easily suppress the 21 cm absorption signal, working against the effect of the AGN radio emission studied in this work. Our models with  $f_{\text{esc}}^{\text{X}} = 1$  produce IGM temperatures much higher than expected for pre-heating by X-ray binaries (Fialkov, Barkana, and Visbal 2014; Eide et al. 2018), with  $T_{\text{K}}$  reaching  $\gtrsim 10^4$  K by  $z = 10$ . These findings indicate that strong 21 cm absorption signals may be difficult to produce in our model unless the production and/or escape of X-ray photons from  $z > 15$  AGN is suppressed.

### 3. Results

#### 3.1 Minimum requirements for the EDGES depth

We begin by considering the minimum requirements to produce a 21 cm signal as deep as that measured by EDGES,  $T_{21} = -500$  mK, by  $z = 17$ . The depth of the absorption signal is maximized if (1) X-ray preheating has not started, such that  $T_{\text{K}}$  is as small as possible, and (2) Ly $\alpha$  coupling is already complete, so that  $T_{\text{S}} = T_{\text{K}}$  (see Eq. 1-2). In this section, we assume these two conditions, and consider what part of our parameter space results in  $T_{21} \leq -500$  mK by  $z = 17$ .

The three most important parameters that affect radio emission in our model are  $f_{\text{bh}}$ ,  $f_{\text{l}}$ , and  $M_{\text{UV}}^{\text{cut}}$  (see Eq. 5). The degenerate combination  $f_{\text{bh}}f_{\text{l}}$ , which we denote  $F_{\text{l}}$ , is the fraction of all objects with  $M_{\text{UV}} < M_{\text{UV}}^{\text{cut}}$  that are radio-loud AGN. The

e. This fortuitous cancellation occurs because the HI cross-section, which dominates the absorption rate, scales like  $\nu^{-2.75} \propto (1+z')^{-2.75}$ , which almost exactly cancels the  $(1+z')^3$  scaling of  $n_{\text{HI}}$  in a neutral IGM.

f. Models with this much pre-heating may even violate measurements of the IGM temperature at  $z < 6$  from the Ly $\alpha$  forest, which find  $T \sim 1-1.5 \times 10^4$  K after reionization (e.g. Boera et al. 2019; Gaikwad et al. 2020).

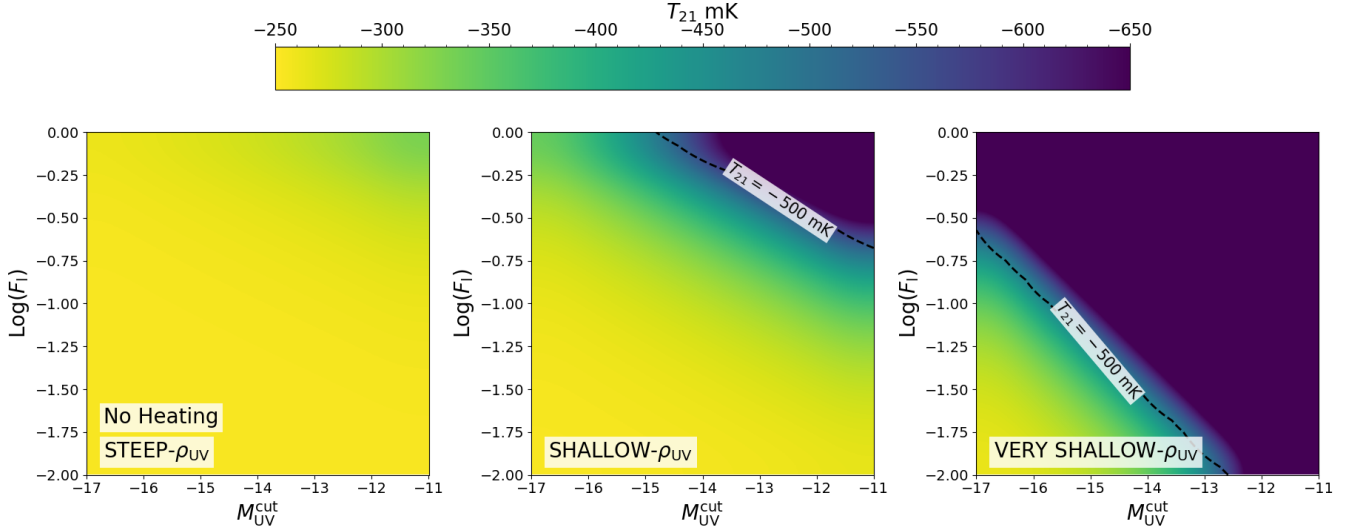


**Figure 4.** Minimum properties of high-redshift AGN required to reach  $T_{21} = -500$  mK by  $z = 17$ . We show  $T_{21}$  at  $z = 17$  vs.  $\log(F_1)$  (vertical axis) and  $M_{\text{UV}}^{\text{cut}}$  (horizontal axis), with the dashed lines denoting  $T_{21} = -500$  mK. These calculations assume complete  $\text{Ly}\alpha$  coupling and no X-ray heating, the most optimistic assumptions for the signal depth. No part of our parameter space in the STEEP- $\rho_{\text{UV}}$  model can reach  $-500$  mK by  $z = 17$ . The SHALLOW- $\rho_{\text{UV}}$  model (middle panel) only does so in the top right corner of parameter space, where nearly all objects down to very faint magnitudes ( $M_{\text{UV}} \gtrsim -14$ ) are radio-loud AGN. Only the VERY SHALLOW- $\rho_{\text{UV}}$  model (right-most panel) can achieve the required depth with  $M_{\text{UV}}^{\text{cut}} \leq -17$  or a radio-loud fraction  $< 10\%$ .

Eddington ratio  $\eta_{\text{edd}}$  also enters Eq. 5 through the conversion from UV luminosity to black hole mass in Eq. 3 and the subsequent conversion to radio luminosity in Eq. 6–7. We find that the dependence of the excess radio background on  $\eta_{\text{edd}}$  is relatively weak – namely, changing  $\eta_{\text{edd}}$  by two orders of magnitude only changes  $T_{21}$  by a factor of  $\sim 2$ . This behavior occurs because  $\eta_{\text{edd}}$  enters through both Equations 3 and 7, and almost cancels out in the conversion from  $L_{\text{UV}}$  to  $L_{5\text{GHz}}$ . Following Hegde, Wyatt, and Furlanetto (2024), we (optimistically) set  $\eta_{\text{edd}} = 1$ , but note that our results are not strongly sensitive to this choice.

In Figure 4, we show  $T_{21}(z = 17)$  vs.  $\log(F_1)$  (vertical axis) and  $M_{\text{UV}}^{\text{cut}}$  (horizontal axis) for each of our three UVLF models assuming an adiabatically cooled IGM and complete  $\text{Ly}\alpha$  coupling. In each panel, the dashed line denotes the iso-contour corresponding to  $T_{21} = -500$  mK. Parts of parameter space above this line – with higher  $F_1$  and/or fainter  $M_{\text{UV}}^{\text{cut}}$  (dark blue regions) – have the potential to reach the absorption depth required by EDGES. Conversely, the green/yellow regions below this line cannot produce EDGES even under the most optimistic circumstances. We see in the left-most panel that no part of parameter space in the STEEP- $\rho_{\text{UV}}$  model can reach  $-500$  mK by  $z = 17$ . Even if *every* UV-bright object were a radio-loud AGN at  $z \geq 17$  down to  $M_{\text{UV}} = -11$  in this model, their combined radio output would be insufficient to backlight EDGES. This model is most consistent with pre-JWST expectations for the UVLF (Oesch et al. 2018) and models that assume constant star formation efficiency in dark matter halos well above  $z = 10$  (Harikane et al. 2023; C. T. Donnan et al. 2025).

The SHALLOW- $\rho_{\text{UV}}$  and VERY SHALLOW- $\rho_{\text{UV}}$  models both produce radio backgrounds large enough to backlight the EDGES depth in some part of our parameter space. The former

requires that either  $\approx 20\%$  of all objects brighter than  $M_{\text{UV}} = -11$  and/or all objects with  $M_{\text{UV}} < -14$  are radio-loud AGN. This is in contrast to observations at lower redshifts, which find that the transition in the UVLF between AGN and stellar-dominated objects should occur at much brighter  $M_{\text{UV}}$  (e.g. Finkelstein and Bagley 2022). A radio-loud fraction near unity is also unexpected, since radio observations of quasars at  $z \lesssim 6$  find radio-loud fractions of order  $\sim 10\%$  or less (E. Bañados et al. 2015; Liu et al. 2021; Keller et al. 2024). In our VERY SHALLOW- $\rho_{\text{UV}}$  model,  $F_1 < 10\%$  is still able to achieve the EDGES depth if  $M_{\text{UV}}^{\text{cut}} < -16$ , and  $M_{\text{UV}}^{\text{cut}} < -17$  is allowed if the radio loud fraction is at least 25%. However, this model requires minimal evolution (an order of magnitude or less) in the UVLF deep into the CD, which would be challenging to reconcile with even the most optimistic galaxy/AGN formation models and observational limits (Yung, Somerville, and Iyer 2025; Castellano et al. 2025; Pérez-González et al. 2025). We note that including the effects of  $\text{Ly}\alpha$  heating would make this result even more pessimistic.

These results show that even under the most optimistic conditions, explaining the depth of the EDGES signal with radio-loud AGN is challenging. Such a scenario requires at least two of three conditions to hold: (1) that the UV luminosity density evolves more gradually than expected at  $z > 15$ , (2) that  $\gtrsim 20\%$  of AGN are radio-loud, in contrast to lower redshift observations, and/or (3) that the majority of objects as faint as  $M_{\text{UV}} = -11$  have their UV light dominated by AGN. In the rest of this work, we will explore the additional conditions required to realize the depth and shape EDGES signal in such a model under less optimistic physical assumptions.



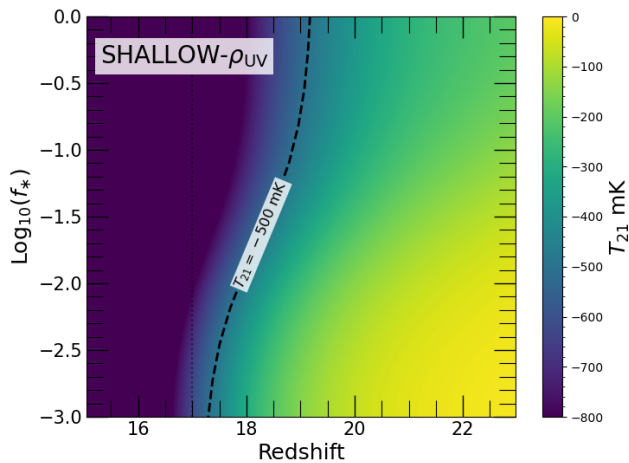


**Figure 5.** Effect of Ly $\alpha$  coupling on the evolution of  $T_{21}$  in our SHALLOW- $\rho_{UV}$  model. We show  $T_{21}$  as a function of  $f_*$  (vertical) and redshift (horizontal) for our most optimistic scenario ( $M_{UV}^{\text{cut}} = -11$  and  $f_1 = f_{\text{bh}} = 1$ ). The dashed line denotes  $T_{21} = -500$  mK, as in Figure 4. The redshift at which  $T_{21} = -500$  mK is reached shifts from  $z = 19.3$  for  $f_* = 1$  to  $z = 17.5$  when  $f_* = 0.001$ . Even our SHALLOW- $\rho_{UV}$  model cannot reach the required EDGES depth without the help of pop III stars to initiate an early onset to Ly $\alpha$  coupling (see text for details).

### 3.2 Additional conditions to achieve the EDGES depth

In this section, we include realistic treatments of Ly $\alpha$  coupling and X-ray heating, and study the conditions required to explain the EDGES depth in our SHALLOW- $\rho_{UV}$  and VERY SHALLOW- $\rho_{UV}$  models. In Figure 5, we illustrate how Ly $\alpha$  coupling affects the depth of the signal by varying the pop III star formation efficiency,  $f_*$  (Eq. 14). The color-scale shows  $T_{21}$  as a function of  $f_*$  (vertical axis) and redshift (horizontal axis), and the dashed line denotes  $T_{21} = -500$  mK, as in Figure 4. The vertical dashed line denotes  $z = 17$ . For this model, we assume  $f_1 = f_{\text{bh}} = 1$  and  $M_{UV}^{\text{cut}} = -11$ , our most optimistic combination of parameters. In the SHALLOW- $\rho_{UV}$  model, lower values of  $f_*$  delay the onset of Ly $\alpha$  coupling, when  $x_\alpha \sim 1$ , to lower redshifts (see top panel of Figure 2). This, in turn, delays the redshift at which  $T_{21}$  reaches the EDGES depth from  $z = 19.3$  (for  $f_* = 1$ ) to  $z = 17.5$  ( $f_* = 0.001$ ). At very low  $f_*$ , the UV photons produced by AGN and pop II stars become the dominant source of Ly $\alpha$  coupling. In this limit, the SHALLOW- $\rho_{UV}$  model barely reaches the EDGES depth by  $z = 17$  in the most optimistic scenario, since UV photons from AGN and pop II stars complete Ly $\alpha$  coupling later than Pop III stars. This is especially problematic given that the flat-bottomed EDGES trough extends to  $z \sim 19.5$ , requiring an earlier completion of Ly $\alpha$  coupling. We note that a smaller value of  $M_{\text{crit}}$  (see discussion in §2.4.2) would help relax the requirements on  $f_*$ .

By contrast, the bottom panel of Figure 2 shows that in the VERY SHALLOW- $\rho_{UV}$  case,  $x_\alpha$  is nearly independent of  $f_*$ , since the bulk of UV photons are produced by AGN and pop II stars. Indeed, in that model the UV production is so high that  $x_\alpha = 1$  is achieved very quickly after  $z = 30$ , and would occur much earlier if we did not impose the condition that

no UV photons are produced at  $z > 30$ . In this model, AGN drive both the coupling of  $T_S$  to the gas temperature and the buildup of the radio background that backlights the signal, such that pop III stars play a minimal role. We thus find that relatively early Ly $\alpha$  coupling by pop III stars is necessary for models like our SHALLOW- $\rho_{UV}$  case to achieve the EDGES depth. Scenarios with higher  $\rho_{UV}$  from AGN and pop II stars at  $z > 15$  can produce a stronger radio background and achieve Ly $\alpha$  coupling by  $z = 17$  without the help of pop III stars.

As outlined in §2.5, AGN are expected to be copious X-ray producers as well as sources of radio photons. X-ray photons pre-heat the IGM, raising  $T_S$  and decreasing the amplitude of the absorption signal. Avoiding this requires that either the X-ray escape fraction ( $f_{\text{esc}}^X$  in Eq. 20) is small, and/or that high-redshift AGN produce fewer high-energy photons than their low-redshift counterparts. The former could be due to e.g. obscuration in the early growth phases of AGN (G. Yang et al. 2023), and the latter may be expected if these super-Eddington accretion is common at these redshifts (Madau et al. 2024). Here, we use  $f_{\text{esc}}^X$  as a proxy for both scenarios.

In Figure 6, we show the conditions on  $f_{\text{esc}}^X$  required to achieve the EDGES absorption depth, in the same format as Figure 5. We assume  $f_* = 0.05$ , as in Figure 2, continue using  $F_1 = 1$  and  $M_{UV}^{\text{cut}} = -11$ . The left and right panels show our SHALLOW- $\rho_{UV}$  and VERY SHALLOW- $\rho_{UV}$  models. We see that they require  $\log(f_{\text{esc}}^X) \approx -2.0$  and  $-1.8$  to achieve the EDGES depth at  $z = 17$ , respectively. This is roughly 1.5 orders of magnitude lower than Lyman Continuum (LyC) escape fractions of  $f_{\text{esc}}^{\text{LyC}} \sim 0.3$  measured for faint AGN at  $z \lesssim 4$  measured by Smith et al. (2020). This discrepancy is exacerbated by the fact that the absorption cross-section of HI is several orders of magnitude smaller for hard X-rays than for LyC photons, suggesting that X-rays should escape AGN more easily than LyC photons (such that  $f_{\text{esc}}^X \geq f_{\text{esc}}^{\text{LyC}}$ ). At  $z \approx 19$ , the maximum  $f_{\text{esc}}^X$  approaches 0 for the SHALLOW- $\rho_{UV}$  model, since that model cannot achieve the EDGES depth by that redshift even in the most optimistic case. In the VERY SHALLOW- $\rho_{UV}$ , it remains nearly constant with redshift.

It is interesting that the maximum value allowed for  $f_{\text{esc}}^X$  to produce the EDGES depth is similar in these two models, despite the fact that the VERY SHALLOW- $\rho_{UV}$  case produces a much stronger radio background (see Figure 4). This insensitivity arises from the fact that the same AGN producing the radio background are also the X-ray producers, such that the ratio of radio to X-ray output does not depend too strongly on the assumed UVLF. Indeed, this coupling is a direct consequence from our use of the quasar fundamental plane to estimate the radio output of AGN directly from their X-ray luminosities (Eq. 6). Thus, a stronger radio background will always be accompanied by more X-ray heating, and the only way to significantly change the relationship between these is via  $f_{\text{esc}}^X$ . Thus, we conclude that an AGN-driven backlight for the EDGES signal demands very low X-ray escape fractions and/or much weaker X-ray production than analogous AGN at lower redshifts, by at least 1.5 orders of magnitude.

In Figure 7, we show examples of scenarios that can reach

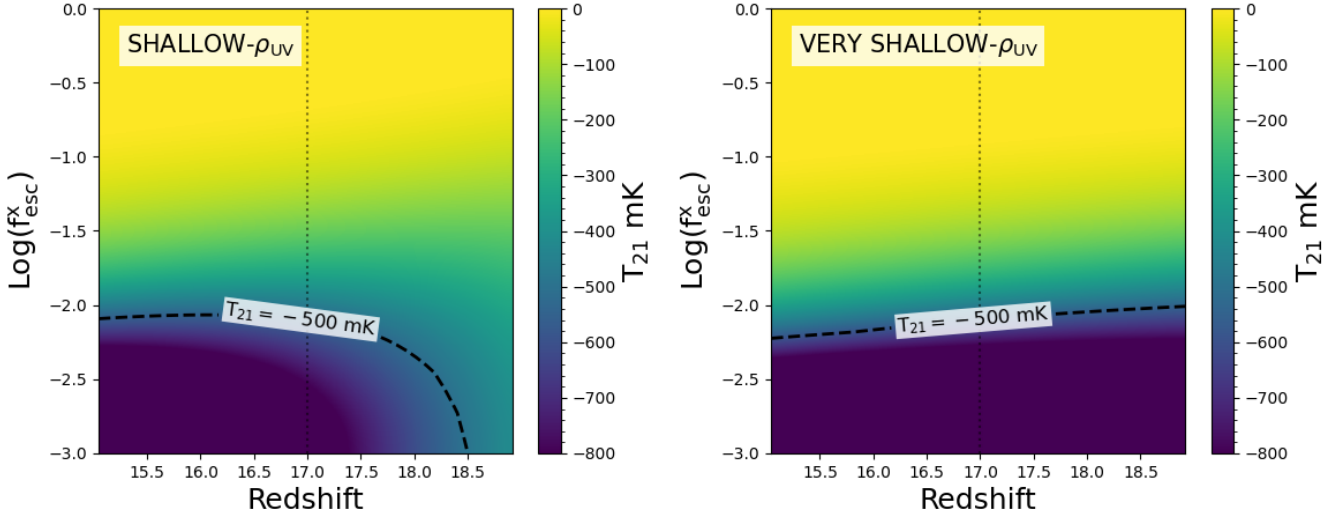


**Figure 6.** Conditions on  $f_{\text{esc}}^{\text{X}}$  required to achieve the EDGES absorption depth. The left and right panels show the SHALLOW- $\rho_{\text{UV}}$  and VERY SHALLOW- $\rho_{\text{UV}}$  models, respectively, and the format is the same as that of Figure 5. We assume  $F_{\text{I}} = 1$  and  $M_{\text{UV}}^{\text{cut}} = -11$ , as in Figure 5. We find that  $\log(f_{\text{esc}}^{\text{X}}) \lesssim -2.5$  ( $\lesssim -2.0$ ) is required to reach  $T_{21} = -500$  mK by  $z \sim 17$  on the left and right, respectively. In the SHALLOW- $\rho_{\text{UV}}$  model, the dashed line drops towards  $f_{\text{esc}}^{\text{X}} = 0$  approaching  $z = 19$ , while in the VERY SHALLOW- $\rho_{\text{UV}}$  case it remains roughly constant with redshift.

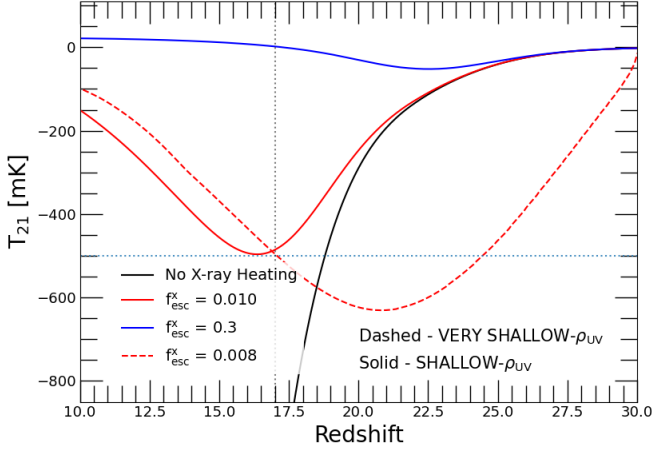


**Figure 7.** Examples of scenarios that produce the  $T_{21} = -500$  mK absorption depth seen by EDGES in the SHALLOW- $\rho_{\text{UV}}$  (red solid) and VERY SHALLOW- $\rho_{\text{UV}}$  (red dashed) models. Both models include Ly $\alpha$  coupling (with  $f_{*} = 0.05$ ). The SHALLOW- $\rho_{\text{UV}}$  and VERY SHALLOW- $\rho_{\text{UV}}$  assume  $f_{\text{esc}}^{\text{X}} = 0.01$  and 0.008, respectively. The black solid curve shows what the SHALLOW- $\rho_{\text{UV}}$  case would look like without any X-ray heating, and the blue solid curve shows the same for a much higher  $f_{\text{esc}}^{\text{X}} = 0.3$ . The SHALLOW- $\rho_{\text{UV}}$  model reaches the target depth slightly too late at  $z \approx 16$ , and the VERY SHALLOW- $\rho_{\text{UV}}$  case, though it goes through  $-500$  mK at  $z = 17$ , reaches it too early at  $z \approx 21$ . See text for discussion.

$T_{21} = -500$  mK in the  $15 < z < 20$  range. The solid and dashed red curves show  $T_{21}$  vs.  $z$  for our SHALLOW- $\rho_{\text{UV}}$  and VERY SHALLOW- $\rho_{\text{UV}}$  models, respectively, for scenarios that include the effects of Ly $\alpha$  coupling (with  $f_{*} = 0.05$ ) and X-ray heating. For the former, we assume  $F_{\text{I}} = 1$  and  $M_{\text{UV}}^{\text{cut}} = -11$ , and the latter we use less extreme values of  $F_{\text{I}} = 0.85$  and

$M_{\text{UV}}^{\text{cut}} = -15$ . Respectively, the two models assume  $f_{\text{esc}}^{\text{X}} = 0.01$  and 0.008, close to the dashed lines in Figure 6. The black solid curve shows the SHALLOW- $\rho_{\text{UV}}$  case in the absence of any X-ray heating, and the blue solid curve shows the same for a much higher  $f_{\text{esc}}^{\text{X}} = 0.3$ , consistent with measurements of  $f_{\text{esc}}^{\text{LyC}}$  by Smith et al. (2020) at much lower redshift. The vertical dotted line indicates  $z = 17$  and the horizontal one denotes  $-500$  mK.

We see that the SHALLOW- $\rho_{\text{UV}}$  model reaches the depth of the EDGES signal slightly too late, at  $z \approx 16$  rather than central  $z = 17$ . This is because X-ray heating, which is needed to produce the up-turn in the signal at lower redshifts, starts at  $z \approx 20$  and reduces the depth of the absorption feature slightly at  $z = 17$ . This up-turn is fairly gradual in our model, with  $T_{21} = -150$  mK by  $z = 10$ . This is due to the ongoing production of radio photons at  $z < 15$ , which makes it more difficult for the signal to saturate (that is, to reach  $T_{\text{S}} \gg T_{\text{radio}}$ ). The blue solid curve shows that much higher X-ray escape washes out the CD signal almost completely. The VERY SHALLOW- $\rho_{\text{UV}}$  model, by contrast, goes through  $-500$  mK at  $z = 17$ , but reaches the EDGES depth early at  $z \approx 21$ , thanks to the rapid early buildup of the radio background and onset of Ly $\alpha$  coupling. In this case, the signal also takes a long time to saturate, reaching  $T_{21} = -100$  mK by  $z = 10$ .

Our findings suggest that achieving the EDGES depth at  $z \sim 17$  with a radio background produced by AGN is challenging even under optimistic assumptions about the radio emission properties of the AGN population. Scenarios with low UV production at  $z > 20$  require a significant early contribution to Ly $\alpha$  coupling from pop III stars to lower  $T_{\text{S}}$  enough to achieve the required depth. In all scenarios, the X-ray escape fraction and/or intrinsic X-ray production of AGN must be at least

$\approx 1.5$  orders of magnitude below low-redshift expectations to avoid washing out the signal via pre-heating. These findings further narrow the parameter space within which AGN could provide the necessary radio backlight to explain EDGES.

### 3.3 Conditions to reproduce the shape of EDGES

In this section, we consider the conditions required for AGN to explain the unexpected shape of the EDGES signal, and not just its depth. The flattened bottom and steep redshift evolution on both sides of the EDGES signal are unexpected in canonical models of the 21 cm CD signal, which prefer less abrupt redshift evolution (Cang et al. 2024). Recently, Mittal and Kulkarni (2022) showed that reproducing these features of EDGES in their model required sharp redshift evolution in the properties of the galaxy population that would be difficult to explain physically. We re-visit this problem in the context of our AGN-driven model here.

One key feature of EDGES is its sharp evolution from near-zero signal at  $z \approx 21.5$  to its maximum depth of  $T_{21} = -500$  mK at  $z \approx 19$ , over a redshift interval of just  $\Delta z \approx 2.5$ . This is hard to reproduce in our models, which generally predict longer redshift intervals ( $\Delta z \approx 5 - 10$ ) between the onset of the signal and maximum depth (see Figure 7). There are two plausible mechanisms that could drive such a fast transition in our model: (1) either  $\text{Ly}\alpha$  coupling happens more rapidly than expected, and/or (2) the excess radio background builds up rapidly  $z < 21.5$ . The problem with (2) is that even absent any excess radio background before  $z = 21.5$ , the CMB alone would be sufficient to backlight absorption at these redshifts if  $\text{Ly}\alpha$  coupling was already underway. We have explored both types of scenarios and find that the high-redshift “edge” of the signal is impossible to fit without an abrupt shutoff of *all* UV sources (AGN, Pop II, and Pop III stars) at  $z > 21.5$ . Note that in our VERY SHALLOW- $\rho_{\text{UV}}$ ,  $\text{Ly}\alpha$  coupling is driven by AGN and Pop II stars rather than Pop III (see Figure 2), such that the main effect of this cutoff is to set  $f_{\text{bh}} = 0$  at  $z > 21.5$ .

We turn next to the rapid saturation of the EDGES signal between  $z \approx 16$  and 14. Assuming  $\text{Ly}\alpha$  coupling is complete by this redshift, we could try to explain this feature by adding redshift evolution to any of our parameters that control the growth of the radio background and/or heating by X-rays. There are two plausible ways to do this: (1) the radio background stops growing at  $z \approx 16$ , allowing  $T_S$  to catch up quickly with  $T_{\text{radio}}$ , and/or (2) X-ray heating increases rapidly at  $z < 16$ , increasing  $T_S$  such that the same result is achieved. Evidence for (1) may already have some observational support. Recently, D’Silva et al. (2023) performed SED fitting on a sample of high-redshift galaxies from the CEERS (Finkelstein et al. 2024b) and JWST-GLASS (Treu et al. 2022) surveys, including fits that allowed some of the observed UV light to originate from AGN. They found that at  $z \approx 5$  and 7.5, they obtained similar results with and without an AGN component in their fits. However, at  $z \approx 10$ , their recovered star formation rate was lower when including the AGN component by up to a factor of  $\approx 2$ , suggesting that AGN could be responsible for up to half the observed UV light at that redshift. This

is consistent with the results of Hegde, Wyatt, and Furlanetto (2024), who found that up to half of the light from  $z > 10$  objects could originate from AGN sources without violating constraints on galaxy morphology.

One interpretation of the D’Silva et al. (2023) results is that they indicate evolution in the brightness cutoff between stellar-dominated and AGN-dominated sources (that is,  $M_{\text{UV}}^{\text{cut}}$ ). Assuming a sharp cutoff between the two populations, the fraction of UV light produced by AGN can be expressed as

$$x_{\text{AGN}} = \frac{\rho_{\text{UV}}^{\text{AGN}}}{\rho_{\text{UV}}^{\text{total}}} = \frac{\int_{-\infty}^{M_{\text{UV}}^{\text{cut}}} dM_{\text{UV}} \frac{dn}{dM_{\text{UV}}} L_{\text{UV}}}{\int_{-\infty}^{-17} dM_{\text{UV}} \frac{dn}{dM_{\text{UV}}} L_{\text{UV}}} \quad (25)$$

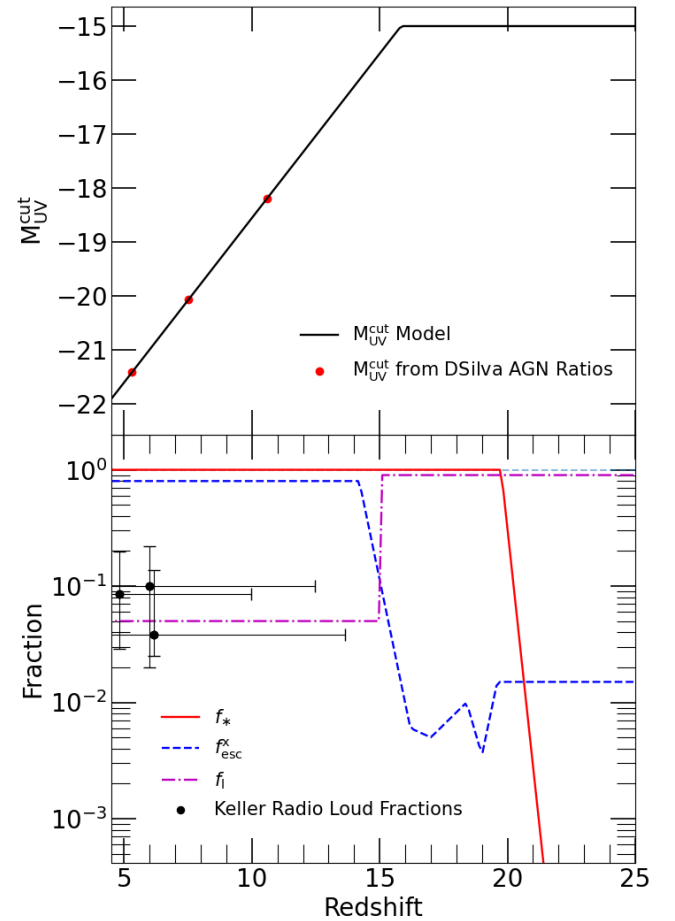


**Figure 8.** Evolution of physical quantities in the scenarios we explore with redshift-dependent parameters. **Top:** our model for evolution in  $M_{\text{UV}}^{\text{cut}}$ , motivated by estimates of the fraction of UV light produced by AGN at  $5 < z < 11$  from D’Silva et al. (2023). The red points are based on measurements from that work (see text), and the black line shows our extrapolation to higher redshifts (capped at  $M_{\text{UV}}^{\text{cut}} = -15$ ). **Bottom:** evolution of  $f_*$  (red),  $f_l$  (magenta) and  $f_{\text{esc}}^{\text{X}}$  (blue) assumed in this section. The black points show recent measurements of the radio-loud fraction of bright quasars at  $5 < z < 6$ , to which our evolving  $f_l$  model is anchored. See text for details.

where the upper limit of  $M_{\text{UV}} = -17$  in the denominator reflects the cutoff used to define  $\rho_{\text{UV}}$  in observations (e.g. Adams et al. (2023)). If we take the ratio of the red and blue points

in the Figure 3 of D’Silva et al. (2023) to be the fraction of light produced by stars ( $1 - x_{\text{AGN}}$ ), we can estimate  $M_{\text{UV}}^{\text{cut}}$  from their data. We perform this exercise and plot the results in the bottom panel of Figure 8. The three red points denote the values of  $M_{\text{UV}}^{\text{cut}}$  inferred in this way from D’Silva et al. (2023) at  $z = 5.5, 7.5$ , and  $10.5$ , which increase linearly with redshift. The black solid line shows a linear extrapolation of these points to higher redshifts, which we cap at  $z = 16$  ( $M_{\text{UV}}^{\text{cut}} = -15$ ). An important caveat is that these results are subject to limited number statistics, especially in the  $z = 10.5$  bin, and should thus be treated with some caution.

We can see that producing enough radio photons to explain EDGES would require significant redshift evolution in  $f_l$  between  $z = 6$  and  $15$ . Measurements of  $f_l$  at  $5 < z < 6$  find values in the 5 – 10% range for bright quasars (E. Bañados et al. 2015; Liu et al. 2021; Keller et al. 2024), far below the  $\gtrsim 25\%$  values required in most of our parameter space to explain EDGES. A rapid transition between  $f_l = 1$  and  $0.05$  around  $z = 15$  would respect these low- $z$  boundary conditions whilst maximally accelerating the saturation of the signal at  $z < 15$ . We show an extreme (step-function) case of such a model as the magenta curve in the bottom panel of Figure 8. The black points denote the measured radio-loud fractions at  $5 < z < 6$  compiled by Keller et al. (2024). The other possibility is that evolution in  $f_{\text{esc}}^X$  drives saturation at  $z \sim 15$ . We showed in Figure 6 that  $f_{\text{esc}}^X \sim 1\%$  is required to produce the EDGES signal depth. However, LyC escape fractions are observed to be  $\sim 30\%$  at  $z \sim 3$  (Smith et al. 2020). Allowing  $f_{\text{esc}}^X$  to evolve rapidly to  $30\%$  at  $z = 15$  could also explain the rapid saturation. We show such a model as the blue curve in Figure 8 (see below for details).

In Figure 9, we show how allowing parameters to evolve affects the signal. The blue dotted curve is the same as the red dashed curve in Figure 7, which assumes constant parameters. The dot-dashed curve includes a sharp cutoff in UV production at  $z > 21.5$ , to achieve rapid onset of Ly $\alpha$  coupling, and our observationally-motivated models for the redshift evolution of  $M_{\text{UV}}^{\text{cut}}$  and  $f_l$  shown in Figure 8, but a constant  $f_{\text{esc}}^X$  that is the same as the blue dotted curve. The red dashed curve adds the evolving  $f_{\text{esc}}^X$  model given by the blue curve in Figure 8, which we have fine-tuned to fit the observed EDGES signal (black solid). We see that although evolving  $M_{\text{UV}}^{\text{cut}}$  and  $f_l$  saturates the signal faster than the “static” case, the absorption profile remains broader than EDGES. This is because a large radio background remains in place even after the sources of radio emission shut off, preventing the signal from vanishing quickly. By contrast, a rapid increase in  $f_{\text{esc}}^X$  drives the IGM temperature well above  $T_{\text{radio}}$  by  $z = 14$ .

We also find that fine-tuning the redshift evolution of  $f_{\text{esc}}^X$  at  $15 < z < 20$  allows us to also reproduce the flat-bottomed shape of the signal. Note that the shape of the dot-dashed magenta curve has a decreasing signal amplitude between its minimum at  $z = 18$  and  $z = 15$ , which does not match EDGES. The local maximum at  $z = 18$  in our evolving  $f_{\text{esc}}^X$  model (blue dashed curve in Figure 8) serves to flatten out this redshift evolution, producing much better agreement. We note that this results achieved with our evolving  $f_{\text{esc}}^X$  could be realized if

some other heating source (such as high-mass X-ray binaries) evolved similarly over this redshift range. Note that although we do not include it here, we expect that Ly $\alpha$  heating (see §2.5) probably would not contribute meaningfully to the heating rate in our best-fitting model. Reis, Fialkov, and Barkana (2021) found that even in optimistic scenario, Ly $\alpha$  and CMB heating can add only a few 10s of K to the gas temperature by  $z = 10$ , while in even our low- $f_{\text{esc}}^X$  models, the gas is a few hundred K by then.

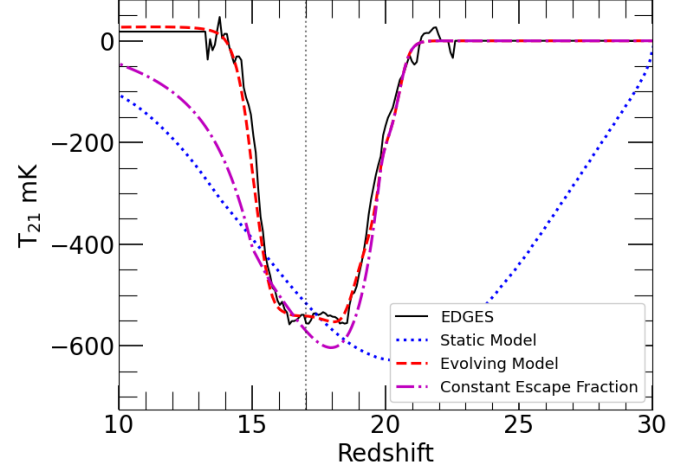


**Figure 9.** Models of  $T_{21}$  with redshift-dependent parameters, compared against the EDGES signal (black solid). The blue dotted curve is our VERY SHALLOW- $\rho_{\text{UV}}$  model with no redshift-dependent parameters from Figure 7. The magenta dot-dashed curve assumes a sharp cutoff in UV emission at  $z > 21.5$ , and the observationally-motivated models for evolving  $M_{\text{UV}}^{\text{cut}}$  and  $f_l$  shown in Figure 8, but retains a constant  $f_{\text{esc}}^X$ . This case comes much closer to the shape of the EDGES signal, but still misses the rapid saturation at  $z \approx 15$  and the flat-bottomed shape of the signal. The red curve uses the evolving  $f_{\text{esc}}^X$  model in Figure 8. By fine-tuning the shape of  $f_{\text{esc}}^X(z)$ , we were able to obtain a good fit to the shape of EDGES.

Lastly, we ask whether the extreme UV emission required by the VERY SHALLOW- $\rho_{\text{UV}}$  model, which is required in our model to reproduce the shape of EDGES is allowed by upper limits on the high-redshift contribution to the near-IR sky surface brightness (SB) from AGN. Based off measurements of the IR-X-Ray cross-correlation (Cappelluti et al. 2013; Kashlinsky et al. 2015; Mitchell-Wynne et al. 2016), Windhorst et al. (2018) argued that the integrated SB at  $2\mu\text{m}$  sourced by Pop III stars and AGN at  $z > 7$  should be  $\gtrsim 31 \text{ mag/arcsec}^2$ , or  $\lesssim 0.04 \text{ nW m}^{-2} \text{ sr}^{-1}$ . For a cutoff of  $M_{\text{UV}}^{\text{cut}} = -11$ , our VERY SHALLOW- $\rho_{\text{UV}}$  has an integrated SB at  $2\mu\text{m}$  of  $0.035 \text{ nW m}^{-2} \text{ sr}^{-1}$  from UV emissions at  $7 < z < 17$ , which is close to this limit. However, there are several reasons that this scenario likely does not violate SB constraints. First, our model only assumes that most UV light is sourced by AGN at  $z \gtrsim 10$ , and integrating down to this redshift gives a SB of only  $0.01 \text{ nW m}^{-2} \text{ sr}^{-1}$ . Second, our best-fitting model in Figure 9 requires only  $M_{\text{UV}}^{\text{cut}} = -15$ , for which we obtain a much more modest  $0.002 \text{ nW m}^{-2} \text{ sr}^{-1}$ , well below the upper limit. Lastly, since these constraints are based on the IR-X-Ray cross-correlation, it is unclear whether they would translate to the same SB limits



in our model, since EDGES requires suppressed X-Ray emission from AGN relative to low-redshift expectations. A full investigation of the IR-X-Ray cross-correlation signal in our scenario is beyond the scope of this work.

Our findings suggest that recovering the shape of the EDGES signal requires, at minimum (1) shallower redshift evolution of the UVLF than in our *SHALLOW- $\rho_{UV}$*  model up to  $z \approx 20$ , (2) a rapid shutoff in UV emission from all sources at  $z > 21.5$  and (3) some evolution in the X-ray escape fraction of high-redshift AGN (or of some other heating source). These results are qualitatively consistent with those of Mittal and Kulkarni (2022). In particular, explored observationally-motivated models for the evolution in AGN abundance and radio emission properties, including evolution in their radio-loud fraction and  $M_{UV}^{cut}$  motivated by radio observations and JWST data at lower redshifts. We found that these models cannot reproduce the rapid saturation and flat-bottomed shape of EDGES without additional help from evolution in X-ray properties.

#### 4. Implications for high-redshift AGN properties

Our findings in the previous section suggest that an AGN-sourced radio background capable of explaining the EDGES signal would require fairly extreme choices of most or all the parameters involved. These include that radio-loud AGN would have to be the dominant sources of UV emission at  $z > 15$ , and have very low production and/or escape of X-ray photons compared to expectations based on lower-redshift expectations. Given these and other extreme requirements discussed above, *it seems unlikely that radio-loud AGN are responsible for EDGES*. Nonetheless, here we briefly speculate about the astrophysical mechanisms that could be at play if this is the case.

The first, most obvious implication of our best-fitting model is that the UVLF transitions from being dominated by galaxies to AGN over the redshift range  $10 \lesssim z \lesssim 15$ . This is the opposite of the trend observed at  $z < 10$ , where the fraction of UV light produced by AGN is observed to decline with redshift (Finkelstein and Bagley 2022). However, it is also qualitatively consistent with observations suggesting that the black hole mass to stellar mass ratio increases with redshift (Ding et al. 2017; Pacucci and Loeb 2024; Maiolino et al. 2024) relative to the canonical relation at  $z = 0$  (Kormendy and Ho 2013). A large population of obscured AGN at high redshifts would also help to explain the abundance of massive quasars at  $z \gtrsim 6$ , which seem to require faster growth rates than suggested by the observed AGN population (Morey et al. 2021; Eilers et al. 2021). Distinguishing these scenarios will require targeted spectroscopic follow-up of high-redshift objects to determine whether faint AGN are ubiquitous in the early universe.

One mechanism that has been proposed to generate an over-abundance of accreting black holes at very high redshift is that of direct collapse (Latif and Ferrara 2016). In this scenario, dissociation of  $H_2$  by the Lyman-Werner background prevents star formation in gas clouds, increasing the Jeans scale and causing gas to collapse directly into a black hole. If direct

collapse black holes (DCBHs) are ubiquitous in the early universe, they could explain the predominance of AGN required in our models. Some recent efforts have been made to identify DCBH candidates at high redshift with JWST (Nabizadeh et al. 2024). Singling out this scenario will require a better understanding of the black hole mass function at high redshifts (Sicilia et al. 2022).

Another implication of our findings is that the production and/or escape of X-ray photons is very low at  $z \gtrsim 15$ , and grows (perhaps abruptly) towards lower redshifts. Evolution in X-ray escape from AGN could be explained if nearly all AGN at very high redshift are highly obscured, by dense HI clouds and/or dust (Gilli et al. 2022; Satyavolu et al. 2023; Mazzolari et al. 2024), which would require an increase in the obscured fraction with redshift (Vijarnwannaluk et al. 2022; Peca et al. 2023). If these AGN are obscured and have low X-ray escape, they would also have low LyC escape fractions, and would likely not start reionization at  $z > 15$ . If escape fractions rapidly increase after this, it may explain the presence of recently-formed ionized bubbles around some UV-luminous sources near this redshift (e.g. Witstok et al. 2025; Naidu et al. 2025). Another possibility is that most AGN at these redshift are in a unique evolutionary stage that enhances their radio production (e.g. Patil et al. 2020) and/or intrinsic X-ray production (Pouliasis et al. 2024).

We briefly comment on the possibility that the AGN responsible for back-lighting EDGES are Little Red Dots (LRDs, Matthee et al. 2024). While the physical nature of LRDs is debated, a number of works have suggested that they could be AGN (Ananna et al. 2024a) that produce little or no X-ray emission (Ananna et al. 2024b; Sacchi and Bogdan 2025). Their lack of X-ray emission may make them a possible candidate to satisfy the conditions described in the previous section. Unfortunately, it is presently unknown whether LRDs emit significantly in the radio (Latif et al. 2025). If LRDs are ever observed to produce significant radio emission, it would warrant a follow-up study similar to this one to determine if they could help explain the EDGES signal.

#### 5. Conclusions

We have investigated the possibility that a population of faint, radio-loud AGN sourced an excess radio background that explains the anomalous depth of the EDGES 21 cm signal. Our main findings are:

- Producing the minimum radio background that can explain the  $\sim 500$  mK depth of the EDGES signal at  $z = 17$  requires that (1) most  $z > 15$  UV luminous objects down to  $M_{UV} = -15$  or fainter are radio-loud AGN, and (2) the redshift evolution of the UVLF up to  $z = 20$  is on the shallow end of what is expected based on the latest JWST measurements at  $10 < z < 14$ .
- Assuming these objects have intrinsic X-ray luminosities comparable to those observed at lower redshifts, the escape fraction of X-ray photons must be  $\lesssim 1\%$  at  $z > 15$  to avoid washing out the signal via X-ray pre-heating. This result



holds regardless of how quickly the UVLF evolves because AGN are sources of both radio and X-ray photons.

- Reproducing the sharp redshift evolution on either side of the EDGES absorption trough requires (1) a rapid decline in UV emission from all sources at  $z > 21.5$  and (2) rapid redshift evolution in the X-ray escape fraction and/or intrinsic X-ray emission of AGN, or of some other heating source such as X-ray binaries. Evolution in the radio emission properties of AGN and their contribution to the UV luminosity function alone cannot reproduce the rapid saturation of the EDGES signal at  $z \sim 15$ .

These extreme requirements render our model an unlikely cosmological explanation for the unexpected depth and shape of the EDGES signal. Our model would suggest that the UVLF transitions from being dominated by stellar sources at  $z \sim 10$  to AGN at  $z \sim 15$  – a cosmic time interval of just  $\approx 200$  Myr (in our cosmology). It would also require the physical conditions dictating X-ray production and/or escape to evolve. These include the fraction of AGN that are obscured by dense HI and/or the detailed physics driving the production of radio and X-ray photons. The requirements of our model will soon be tested by the UV, radio, and X-ray properties of high-redshift galaxies and AGN.

**Acknowledgments** The authors thank Sahil Hegde, Steven Furlanetto, Anson D'Aloisio, and Timothy Carleton for helpful discussions and/or comments on the draft version of this manuscript.

**Funding Statement** AN acknowledges the support of the RENTU program at Arizona State University. CC was supported by the Beus Center for Cosmic Foundations. RAW acknowledges support from NASA/JWST Interdisciplinary Scientist grants NAG5-12460, NNX14AN10G and 80NSSC18K0200 from GSFC.

**Competing Interests** The authors are not aware of any competing interests connected to this work.

**Data Availability Statement** The data underlying this article will be shared upon reasonable request to the corresponding author.

**Ethical Standards** The research meets all ethical guidelines, including adherence to the legal requirements of the study country.

**Author Contributions** AN wrote code, ran calculations, made figures, and helped draft the manuscript. CC provided project guidance, helped check code, and contributed heavily to the drafting of the manuscript. JDS, JB, and RW provided project guidance and feedback on the manuscript.

## References

- Adams, Nathan J., Christopher J. Conselice, Duncan Austin, Thomas Harvey, Leonardo Ferreira, James Trussler, Ignas Juodzbališ, et al. 2023. EPOCHS Paper II: The Ultraviolet Luminosity Function from  $7.5 < z < 13.5$  using 110 square arcminutes of deep, blank-field data from the PEARLS Survey and Public Science Programmes. *arXiv e-prints* (April): arXiv:2304.13721. <https://doi.org/10.48550/arXiv.2304.13721>. arXiv: 2304.13721 [astro-ph.GA].
- Ananna, Tonima Tasnim, Ákos Bogdán, Orsolya E. Kovács, Priyamvada Natarajan, and Ryan C. Hickox. 2024a. X-Ray View of Little Red Dots: Do They Host Supermassive Black Holes? *ApJ* 969, no. 1 (July): L18. <https://doi.org/10.3847/2041-8213/ad5669>. arXiv: 2404.19010 [astro-ph.GA].
- . 2024b. X-Ray View of Little Red Dots: Do They Host Supermassive Black Holes? *ApJ* 969, no. 1 (July): L18. <https://doi.org/10.3847/2041-8213/ad5669>. arXiv: 2404.19010 [astro-ph.GA].
- Bañados, E., B. P. Venemans, E. Morganson, J. Hodge, R. Decarli, F. Walter, D. Stern, et al. 2015. Constraining the Radio-loud Fraction of Quasars at  $z > 5.5$ . *ApJ* 804, no. 2 (May): 118. <https://doi.org/10.1088/0004-637X/804/2/118>. arXiv: 1503.04214 [astro-ph.GA].
- Bañados, Eduardo, Bram P. Venemans, Chiara Mazzucchelli, Emanuele P. Farina, Fabian Walter, Feige Wang, Roberto Decarli, et al. 2018. An 800-million-solar-mass black hole in a significantly neutral Universe at a redshift of 7.5. *Nature* 553, no. 7689 (January): 473–476. <https://doi.org/10.1038/nature25180>. arXiv: 1712.01860 [astro-ph.GA].
- Bariuan, Luis Gabriel C., Bradford Snios, Małgosia Sobolewska, Aneta Siemigłowska, and Daniel A. Schwartz. 2022. The Fundamental Planes of black hole activity for radio-loud and radio-quiet quasars. *MNRAS* 513, no. 4 (July): 4673–4681. <https://doi.org/10.1093/mnras/stac1153>. arXiv: 2201.04666 [astro-ph.HE].
- Bennett, Jake S., Debora Sijacki, Tiago Costa, Nicolas Laporte, and Callum Witten. 2024. The growth of the gargantuan black holes powering high-redshift quasars and their impact on the formation of early galaxies and protoclusters. *Monthly Notices of the Royal Astronomical Society* 527, no. 1 (January): 1033–1054. <https://doi.org/10.1093/mnras/stad3179>. arXiv: 2305.11932 [astro-ph.GA].
- Berkhout, Lindsay M., Daniel C. Jacobs, Zuhra Abdurashidova, Tyrone Adams, James E. Aguirre, Paul Alexander, Zaki S. Ali, et al. 2024. Hydrogen Epoch of Reionization Array (HERA) Phase II Deployment and Commissioning. *PASP* 136, no. 4 (April): 045002. <https://doi.org/10.1088/1538-3873/ad3122>. arXiv: 2401.04304 [astro-ph.IM].
- Bevins, H. T. J., A. Fialkov, E. de Lera Acedo, W. J. Handley, S. Singh, R. Subrahmanyan, and R. Barkana. 2022. Astrophysical constraints from the SARAS 3 non-detection of the cosmic dawn sky-averaged 21-cm signal. *Nature Astronomy* 6 (December): 1473–1483. <https://doi.org/10.1038/s41550-022-01825-6>. arXiv: 2212.00464 [astro-ph.CO].
- Boera, Elisa, George D. Becker, James S. Bolton, and Fahad Nasir. 2019. Revealing Reionization with the Thermal History of the Intergalactic Medium: New Constraints from the Ly $\alpha$  Flux Power Spectrum. *The Astrophysical Journal* 872, no. 1 (February): 101. <https://doi.org/10.3847/1538-4357/aafec4>. arXiv: 1809.06980 [astro-ph.CO].
- Bowler, R A A, M J Jarvis, J S Dunlop, R J McLure, D J McLeod, N J Adams, B Milvang-Jensen, and H J McCracken. 2020. A lack of evolution in the very bright end of the galaxy luminosity function from  $z \approx 8$  to 10. *Monthly Notices of the Royal Astronomical Society* 493, no. 2 (February): 2059–2084. issn: 0035-8711. <https://doi.org/10.1093/mnras/staa313>. eprint: <https://academic.oup.com/mnras/article-pdf/493/2/2059/32738648/staa313.pdf>. <https://doi.org/10.1093/mnras/staa313>.
- Bowler, R. A. A., J. S. Dunlop, R. J. McLure, and D. J. McLeod. 2016. Unveiling the nature of bright  $z \approx 7$  galaxies with the Hubble Space Telescope. *Monthly Notices of the Royal Astronomical Society* 466, no. 3 (December): 3612–3635. issn: 0035-8711. <https://doi.org/10.1093/mnras/stw3296>. eprint: <https://academic.oup.com/mnras/article-pdf/466/3/3612/10904198/stw3296.pdf>. <https://doi.org/10.1093/mnras/stw3296>.

- Bowman, Judd D., Miguel F. Morales, and Jacqueline N. Hewitt. 2007. Constraints on Fundamental Cosmological Parameters with Upcoming Redshifted 21 cm Observations. *The Astrophysical Journal* 661, no. 1 (May): 1–9. <https://doi.org/10.1086/516560>. arXiv: astro-ph/0512262 [astro-ph].
- Bowman, Judd D., Alan E. E. Rogers, Raul A. Monsalve, Thomas J. Mozdzen, and Nivedita Mahesh. 2018. An absorption profile centred at 78 megahertz in the sky-averaged spectrum. *Nature* 555, no. 7694 (March): 67–70. <https://doi.org/10.1038/nature25792>. arXiv: 1810.05912 [astro-ph.CO].
- Boylan-Kolchin, Michael. 2023. Stress testing  $\Lambda$ CDM with high-redshift galaxy candidates. *Nature Astronomy* 7 (June): 731–735. <https://doi.org/10.1038/s41550-023-01937-7>. arXiv: 2208.01611 [astro-ph.CO].
- Cang, Junsong, Andrei Mesinger, Steven G. Murray, Daniela Breitman, Yuxiang Qin, and Roberto Trotta. 2024. The EDGES measurement disfavors an excess radio background during the cosmic dawn. *arXiv e-prints* (November): arXiv:2411.08134. <https://doi.org/10.48550/arXiv.2411.08134>. arXiv: 2411.08134 [astro-ph.CO].
- Cappelluti, N., A. Kashlinsky, R. G. Arendt, A. Comastri, G. G. Fazio, A. Finoguenov, G. Hasinger, J. C. Mather, T. Miyaji, and S. H. Moseley. 2013. Cross-correlating Cosmic Infrared and X-Ray Background Fluctuations: Evidence of Significant Black Hole Populations among the CIB Sources. *ApJ* 769, no. 1 (May): 68. <https://doi.org/10.1088/0004-637X/769/1/68>. arXiv: 1210.5302 [astro-ph.CO].
- Castellano, M., A. Fontana, E. Merlin, P. Santini, L. Napolitano, N. Menci, A. Calabrò, et al. 2025. Pushing JWST to the extremes: search and scrutiny of bright galaxy candidates at  $z \approx 15$ –30. *arXiv e-prints* (April): arXiv:2504.05893. <https://doi.org/10.48550/arXiv.2504.05893>. arXiv: 2504.05893 [astro-ph.GA].
- Chemerynska, Iryna, Hakim Atek, Lukas J. Furtak, Adi Zitrin, Jenny E. Greene, Pratika Dayal, Andrea Weibel, et al. 2024. JWST UNCOVER: the overabundance of ultraviolet-luminous galaxies at  $z > 9$ . *Monthly Notices of the Royal Astronomical Society* 531, no. 2 (June): 2615–2625. <https://doi.org/10.1093/mnras/stae1260>. arXiv: 2312.05030 [astro-ph.GA].
- Chuzhoy, Leonid, Marcelo A. Alvarez, and Paul R. Shapiro. 2006. Recognizing the First Radiation Sources through Their 21 cm Signature. *The Astrophysical Journal* 648, no. 1 (September): L1–L4. <https://doi.org/10.1086/507626>. arXiv: astro-ph/0605511 [astro-ph].
- Cruz, Hector Afonso G., Julian B. Munoz, Nashwan Sabti, and Marc Kamionkowski. 2024. The First Billion Years in Seconds: An Effective Model for the 21-cm Signal with Population III Stars. *arXiv e-prints* (July): arXiv:2407.18294. <https://doi.org/10.48550/arXiv.2407.18294>. arXiv: 2407.18294 [astro-ph.CO].
- D'Silva, Jordan C. J., Simon P. Driver, Claudia D. P. Lagos, Aaron S. G. Robotham, Nathan J. Adams, Christopher J. Conselice, Brenda Frye, et al. 2025. Self-Consistent JWST Census of Star Formation and AGN activity at  $z=5.5$ –13.5. *arXiv e-prints* (March): arXiv:2503.03431. <https://doi.org/10.48550/arXiv.2503.03431>. arXiv: 2503.03431 [astro-ph.GA].
- D'Silva, Jordan C. J., Simon P. Driver, Claudia D. P. Lagos, Aaron S. G. Robotham, Jake Summers, and Rogier A. Windhorst. 2023. Star Formation and AGN Activity 500 Myr after the Big Bang: Insights from JWST. *The Astrophysical Journal* 959, no. 2 (December): L18. <https://doi.org/10.3847/2041-8213/ad103e>. arXiv: 2310.03081 [astro-ph.GA].
- Datta, Kanan K., Somnath Bharadwaj, and T. Roy Choudhury. 2007. Detecting ionized bubbles in redshifted 21-cm maps. *Monthly Notices of the Royal Astronomical Society* 382, no. 2 (December): 809–818. <https://doi.org/10.1111/j.1365-2966.2007.12421.x>. arXiv: astro-ph/0703677 [astro-ph].
- Datta, Kanan K., Aritra Kundu, Ankit Paul, and Ankita Bera. 2020. Cosmic recombination history in light of EDGES measurements of the cosmic dawn 21-cm signal. *Phys. Rev. D* 102, no. 8 (October): 083502. <https://doi.org/10.1103/PhysRevD.102.083502>. arXiv: 2001.06497 [astro-ph.CO].
- Ding, Xuheng, Tommaso Treu, Sherry H. Suyu, Kenneth C. Wong, Takahiro Morishita, Daeseong Park, Dominique Sluse, et al. 2017. H0LiCOW VII: cosmic evolution of the correlation between black hole mass and host galaxy luminosity. *MNRAS* 472, no. 1 (November): 90–103. <https://doi.org/10.1093/mnras/stx1972>. arXiv: 1703.02041 [astro-ph.GA].
- Donnan, C T, D J McLeod, J S Dunlop, R J McLure, A C Carnall, R Begley, F Cullen, et al. 2022. The evolution of the galaxy UV luminosity function at redshifts  $z \approx 8$ –15 from deep JWST and ground-based near-infrared imaging. *Monthly Notices of the Royal Astronomical Society* 518, no. 4 (November): 6011–6040. issn: 0035-8711. <https://doi.org/10.1093/mnras/stac3472>. eprint: <https://academic.oup.com/mnras/article-pdf/518/4/6011/47887826/stac3472.pdf>. <https://doi.org/10.1093/mnras/stac3472>.
- Donnan, C T, R J McLure, J S Dunlop, D J McLeod, D Magee, K Z Arellano-Córdova, L Barrufet, et al. 2024. Jwst primer: a new multifield determination of the evolving galaxy uv luminosity function at redshifts  $z \approx 9$ –15. *Monthly Notices of the Royal Astronomical Society* 533, no. 3 (August): 3222–3237. issn: 0035-8711. <https://doi.org/10.1093/mnras/stae2037>. eprint: <https://academic.oup.com/mnras/article-pdf/533/3/3222/59054112/stae2037.pdf>. <https://doi.org/10.1093/mnras/stae2037>.
- Donnan, C. T., J. S. Dunlop, R. J. McLure, D. J. McLeod, and F. Cullen. 2025. No evidence (yet) for increased star-formation efficiency at early times. *arXiv e-prints* (January): arXiv:2501.03217. <https://doi.org/10.48550/arXiv.2501.03217>. arXiv: 2501.03217 [astro-ph.GA].
- Duras, F., A. Bongiorno, F. Ricci, E. Piconcelli, F. Shankar, E. Lusso, S. Bianchi, et al. 2020. Universal bolometric corrections for active galactic nuclei over seven luminosity decades. *A&A* 636 (April): A73. <https://doi.org/10.1051/0004-6361/201936817>. arXiv: 2001.09984 [astro-ph.GA].
- Eide, Marius B, Luca Graziani, Benedetta Ciardi, Yu Feng, Koki Kakiichi, and Tiziana Di Matteo. 2018. The epoch of cosmic heating by early sources of x-rays. *Monthly Notices of the Royal Astronomical Society* 476, no. 1 (February): 1174–1190. issn: 0035-8711. <https://doi.org/10.1093/mnras/sty272>. eprint: <https://academic.oup.com/mnras/article-pdf/476/1/1174/24261079/sty272.pdf>. <https://doi.org/10.1093/mnras/sty272>.
- Eilers, Anna-Christina, Frederick B. Davies, and Joseph F. Hennawi. 2018. The Opacity of the Intergalactic Medium Measured along Quasar Sightlines at  $z \approx 6$ . *The Astrophysical Journal* 864, no. 1 (September): 53. <https://doi.org/10.3847/1538-4357/aad4fd>. arXiv: 1807.04229 [astro-ph.GA]. <https://ui.adsabs.harvard.edu/abs/2018ApJ...864...53E>.
- Eilers, Anna-Christina, Joseph F. Hennawi, Frederick B. Davies, and Robert A. Simcoe. 2021. Detecting and Characterizing Young Quasars. II. Four Quasars at  $z \approx 6$  with Lifetimes  $< 10^4$  Yr. *ApJ* 917, no. 1 (August): 38. <https://doi.org/10.3847/1538-4357/ac0a76>. arXiv: 2106.04586 [astro-ph.GA].
- Ewall-Wice, A., T. -C. Chang, J. Lazio, O. Doré, M. Seiffert, and R. A. Monsalve. 2018. Modeling the Radio Background from the First Black Holes at Cosmic Dawn: Implications for the 21 cm Absorption Amplitude. *The Astrophysical Journal* 868, no. 1 (November): 63. <https://doi.org/10.3847/1538-4357/aae51d>. arXiv: 1803.01815 [astro-ph.CO].
- Ewall-Wice, Aaron, Tzu-Ching Chang, and T. Joseph W. Lazio. 2020. The Radio Scream from black holes at Cosmic Dawn: a semi-analytic model for the impact of radio-loud black holes on the 21 cm global signal. *Monthly Notices of the Royal Astronomical Society* 492, no. 4 (March): 6086–6104. <https://doi.org/10.1093/mnras/stz3501>. arXiv: 1903.06788 [astro-ph.GA].
- Fialkov, Anastasia, Rennan Barkana, and Eli Visbal. 2014. The observable signature of late heating of the Universe during cosmic reionization. *Nature* 506, no. 7487 (February): 197–199. <https://doi.org/10.1038/nature12999>. arXiv: 1402.0940 [astro-ph.CO]. <https://ui.adsabs.harvard.edu/abs/2014Natur.506..197F>.
- Field, George B. 1958. Excitation of the Hydrogen 21-CM Line. *Proceedings of the IRE* 46 (January): 240–250. <https://doi.org/10.1109/JRPROC.1958.286741>.

- Finkelstein, Steven L., and Micaela B. Bagley. 2022. On the Coevolution of the AGN and Star-forming Galaxy Ultraviolet Luminosity Functions at  $3 < z < 9$ . *The Astrophysical Journal* 938, no. 1 (October): 25. <https://doi.org/10.3847/1538-4357/ac89eb>. arXiv: 2207.02233 [astro-ph.GA].
- Finkelstein, Steven L., Gene C. K. Leung, Micaela B. Bagley, Mark Dickinson, Henry C. Ferguson, Casey Papovich, Hollis B. Akins, et al. 2024a. The Complete CEERS Early Universe Galaxy Sample: A Surprisingly Slow Evolution of the Space Density of Bright Galaxies at  $z \sim 8.5$ –14.5. *The Astrophysical Journal* 969, no. 1 (July): L2. <https://doi.org/10.3847/2041-8213/ad4495>. arXiv: 2311.04279 [astro-ph.GA].
- . 2024b. The Complete CEERS Early Universe Galaxy Sample: A Surprisingly Slow Evolution of the Space Density of Bright Galaxies at  $z \sim 8.5$ –14.5. *The Astrophysical Journal* 969, no. 1 (July): L2. <https://doi.org/10.3847/2041-8213/ad4495>. arXiv: 2311.04279 [astro-ph.GA].
- Fixsen, D. J., A. Kogut, S. Levin, M. Limon, P. Lubin, P. Mirel, M. Seiffert, et al. 2011. ARCADE 2 Measurement of the Absolute Sky Brightness at 3–90 GHz. *The Astrophysical Journal* 734, no. 1 (June): 5. <https://doi.org/10.1088/0004-637X/734/1/5>. arXiv: 0901.0555 [astro-ph.CO].
- Fujimoto, Seiji, Rohan P. Naidu, John Chisholm, Hakim Atek, Ryan Endsley, Vasily Kokorev, Lukas J. Furtak, et al. 2025. GLIMPSE: An ultra-faint  $\approx 10^5 M_\odot$  Pop III Galaxy Candidate and First Constraints on the Pop III UV Luminosity Function at  $z \approx 6$ –7. *arXiv e-prints* (January): arXiv:2501.11678. <https://doi.org/10.48550/arXiv.2501.11678>. arXiv: 2501.11678 [astro-ph.GA].
- Furlanetto, Steven R. 2006. The global 21-centimeter background from high redshifts. *MNRAS* 371, no. 2 (September): 867–878. <https://doi.org/10.1111/j.1365-2966.2006.10725.x>. arXiv: astro-ph/0604040 [astro-ph].
- Gaikwad, Prakash, Michael Rauch, Martin G. Haehnelt, Ewald Puchwein, James S. Bolton, Laura C. Keating, Girish Kulkarni, et al. 2020. Probing the thermal state of the intergalactic medium at  $z > 5$  with the transmission spikes in high-resolution Ly  $\alpha$  forest spectra. *Monthly Notices of the Royal Astronomical Society* 494, no. 4 (June): 5091–5109. <https://doi.org/10.1093/mnras/staa907>. arXiv: 2001.10018 [astro-ph.CO].
- Gilli, R., C. Norman, F. Calura, F. Vito, R. Decarli, S. Marchesi, K. Iwasawa, et al. 2022. Supermassive black holes at high redshift are expected to be obscured by their massive host galaxies' interstellar medium. *A&A* 666 (October): A17. <https://doi.org/10.1051/0004-6361/202243708>. arXiv: 2206.03508 [astro-ph.GA].
- Giri, Sambit K., Anson D'Aloisio, Garrelt Mellema, Eiichi Komatsu, Raghu-nath Ghara, and Suman Majumdar. 2019. Position-dependent power spectra of the 21-cm signal from the epoch of reionization. *Journal of Cosmology and Astro-Particle Physics* 2019, no. 2 (February): 058. <https://doi.org/10.1088/1475-7516/2019/02/058>. arXiv: 1811.09633 [astro-ph.CO]. <https://ui.adsabs.harvard.edu/abs/2019JCAP...02..058G>.
- Gloudemans, A. J., K. J. Duncan, A. Saxena, Y. Harikane, G. J. Hill, G. R. Zeimann, H. J. A. Röttgering, et al. 2022. Discovery of 24 radio-bright quasars at  $4.9 \leq z \leq 6.6$  using low-frequency radio observations. *A&A* 668 (December): A27. <https://doi.org/10.1051/0004-6361/202244763>. arXiv: 2210.01811 [astro-ph.GA].
- Gnedin, Nickolay Y., and Peter A. Shaver. 2004. Redshifted 21 Centimeter Emission from the Pre-Reionization Era. I. Mean Signal and Linear Fluctuations. *The Astrophysical Journal* 608, no. 2 (June): 611–621. <https://doi.org/10.1086/420735>. arXiv: astro-ph/0312005 [astro-ph].
- Halder, Ashadul, and Shibaji Banerjee. 2021. Bounds on abundance of primordial black hole and dark matter from EDGES 21-cm signal. *Phys. Rev. D* 103, no. 6 (March): 063044. <https://doi.org/10.1103/PhysRevD.103.063044>. arXiv: 2102.00959 [astro-ph.CO].
- Harikane, Yuichi, Akio K. Inoue, Richard S. Ellis, Masami Ouchi, Yurina Nakazato, Naoki Yoshida, Yoshiaki Ono, et al. 2025. JWST, ALMA, and Keck Spectroscopic Constraints on the UV Luminosity Functions at  $z \sim 7$ –14: Clumpiness and Compactness of the Brightest Galaxies in the Early Universe. *The Astrophysical Journal* 980, no. 1 (February): 138. <https://doi.org/10.3847/1538-4357/ad9b2c>. arXiv: 2406.18352 [astro-ph.GA].
- Harikane, Yuichi, Masami Ouchi, Masamune Oguri, Yoshiaki Ono, Kimihiko Nakajima, Yuki Isobe, Hiroya Umeda, Ken Mawatari, and Yechi Zhang. 2023. A Comprehensive Study of Galaxies at  $z$  9–16 Found in the Early JWST Data: Ultraviolet Luminosity Functions and Cosmic Star Formation History at the Pre-reionization Epoch. *ApJS* 265, no. 1 (March): 5. <https://doi.org/10.3847/1538-4365/acaa9>. arXiv: 2208.01612 [astro-ph.GA].
- Hegde, Sahil, and Steven R. Furlanetto. 2023. A self-consistent semi-analytic model for Population III star formation in minihaloes. *MNRAS* 525, no. 1 (October): 428–447. <https://doi.org/10.1093/mnras/stad2308>. arXiv: 2304.03358 [astro-ph.CO].
- Hegde, Sahil, Michael M. Wyatt, and Steven R. Furlanetto. 2024. A hidden population of active galactic nuclei can explain the overabundance of luminous  $z > 10$  objects observed by JWST. *Journal of Cosmology and Astroparticle Physics* 2024, no. 8 (August): 025. <https://doi.org/10.1088/1475-7516/2024/08/025>. arXiv: 2405.01629 [astro-ph.GA].
- HERA Collaboration, Zara Abdurashidova, Tyrone Adams, James E. Aguirre, Paul Alexander, Zaki S. Ali, Rushelle Baartman, et al. 2023. Improved Constraints on the 21 cm EoR Power Spectrum and the X-Ray Heating of the IGM with HERA Phase I Observations. *ApJ* 945, no. 2 (March): 124. <https://doi.org/10.3847/1538-4357/acaf50>. arXiv: 2210.04912 [astro-ph.CO].
- Hibbard, Joshua J., Jordan Mirocha, David Rapetti, Neil Bassett, Jack O. Burns, and Keith Tauscher. 2022. Constraining Warm Dark Matter and Population III Stars with the Global 21 cm Signal. *The Astrophysical Journal* 929, no. 2 (April): 151. <https://doi.org/10.3847/1538-4357/ac5ea3>. arXiv: 2201.02638 [astro-ph.CO].
- Hills, Richard, Girish Kulkarni, P. Daniel Meerburg, and Ewald Puchwein. 2018. Concerns about modelling of the EDGES data. *Nature* 564, no. 7736 (December): E32–E34. <https://doi.org/10.1038/s41586-018-0796-5>. arXiv: 1805.01421 [astro-ph.CO].
- Hirata, Christopher M. 2006. Wouthuysen-Field coupling strength and application to high-redshift 21-cm radiation. *MNRAS* 367, no. 1 (March): 259–274. <https://doi.org/10.1111/j.1365-2966.2005.09949.x>. arXiv: astro-ph/0507102 [astro-ph].
- Jeong, Tae Bong, Myoungwon Jeon, Hyunmi Song, and Volker Bromm. 2025. Simulating High-redshift Galaxies: Enhancing UV Luminosity with Star Formation Efficiency and a Top-heavy IMF. *The Astrophysical Journal* 980, no. 1 (February): 10. <https://doi.org/10.3847/1538-4357/ada27d>. arXiv: 2411.17007 [astro-ph.GA].
- Johnson, Jarrett Lawrence, and Phoebe R. Upton Sanderbeck. 2022. A Simple Condition for Sustained Super-Eddington Black Hole Growth. *The Astrophysical Journal* 934, no. 1 (July): 58. <https://doi.org/10.3847/1538-4357/ac7b81>. arXiv: 2201.11757 [astro-ph.GA].
- Kashlinsky, A., J. C. Mather, K. Helgason, R. G. Arendt, V. Bromm, and S. H. Moseley. 2015. Reconstructing Emission from Pre-reionization Sources with Cosmic Infrared Background Fluctuation Measurements by the JWST. *ApJ* 804, no. 2 (May): 99. <https://doi.org/10.1088/0004-637X/804/2/99>. arXiv: 1412.5566 [astro-ph.CO].
- Keller, Pascal M., Nithyanandan Thyagarajan, Ajay Kumar, Nissim Kanekar, and Gianni Bernardi. 2024. The radio-loud fraction of quasars at  $z > 6$ . *MNRAS* 528, no. 4 (March): 5692–5702. <https://doi.org/10.1093/mnras/stae418>. arXiv: 2402.08732 [astro-ph.GA].

- Koopmans, L., J. Pritchard, G. Mellema, J. Aguirre, K. Ahn, R. Barkana, I. van Bemmel, et al. 2015. The Cosmic Dawn and Epoch of Reionisation with SKA. In *Advancing astrophysics with the square kilometre array (aaska14)*, 1. April. <https://doi.org/10.22323/1.215.0001>. arXiv: 1505.07568 [astro-ph.CO].
- Kormendy, John, and Luis C. Ho. 2013. Coevolution (Or Not) of Supermassive Black Holes and Host Galaxies. *ARA&A* 51, no. 1 (August): 511–653. <https://doi.org/10.1146/annurev-astro-082708-101811>. arXiv: 1304.7762 [astro-ph.CO].
- Kulkarni, Mihir, Eli Visbal, and Greg L. Bryan. 2021. The Critical Dark Matter Halo Mass for Population III Star Formation: Dependence on Lyman-Werner Radiation, Baryon-dark Matter Streaming Velocity, and Redshift. *ApJ* 917, no. 1 (August): 40. <https://doi.org/10.3847/1538-4357/ac08a3>. arXiv: 2010.04169 [astro-ph.GA].
- Latif, Muhammad A., Ammara Aftab, Daniel J. Whalen, and Mar Mezcuca. 2025. Radio emission from little red dots may reveal their true nature. *A&A* 694 (February): L14. <https://doi.org/10.1051/0004-6361/202453194>. arXiv: 2502.03742 [astro-ph.GA].
- Latif, Muhammad A., and Andrea Ferrara. 2016. Formation of Supermassive Black Hole Seeds. *PASA* 33 (October): e051. <https://doi.org/10.1017/pasa.2016.41>. arXiv: 1605.07391 [astro-ph.GA].
- Liu, Yuanqi, Ran Wang, Emmanuel Momjian, Eduardo Bañados, Greg Zeimann, Chris J. Willott, Yoshiki Matsuoka, et al. 2021. Constraining the Quasar Radio-loud Fraction at  $z \sim 6$  with Deep Radio Observations. *ApJ* 908, no. 2 (February): 124. <https://doi.org/10.3847/1538-4357/abd3a8>. arXiv: 2012.07301 [astro-ph.GA].
- Long, Qing-Chen, Ai-Jun Dong, Qi-Jun Zhi, and Lun-Hua Shang. 2025. Revisiting the Fundamental Planes of Black Hole Activity for Strong Jet Sources. *The Astrophysical Journal* 980, no. 2 (February): 187. <https://doi.org/10.3847/1538-4357/adaae>. arXiv: 2501.11381 [astro-ph.HE].
- Lu, Shengdong, Carlos S. Frenk, Sownak Bose, Cedric G. Lacey, Shaun Cole, Carlton M. Baugh, and John C. Helly. 2025. A comparison of pre-existing  $\Lambda$ CDM predictions with the abundance of JWST galaxies at high redshift. *Monthly Notices of the Royal Astronomical Society* 536, no. 1 (January): 1018–1034. <https://doi.org/10.1093/mnras/stae2646>. arXiv: 2406.02672 [astro-ph.GA].
- Lusso, E., A. Comastri, B. D. Simmons, M. Mignoli, G. Zamorani, C. Vignali, M. Brusa, et al. 2012. Bolometric luminosities and Eddington ratios of X-ray selected active galactic nuclei in the XMM-COSMOS survey. *MNRAS* 425, no. 1 (September): 623–640. <https://doi.org/10.1111/j.1365-2966.2012.21513.x>. arXiv: 1206.2642 [astro-ph.CO].
- Lusso, E., A. Comastri, C. Vignali, G. Zamorani, M. Brusa, R. Gilli, K. Iwasawa, et al. 2010. The X-ray to optical-UV luminosity ratio of X-ray selected type 1 AGN in XMM-COSMOS. *Astronomy & Astrophysics* 512 (March): A34. <https://doi.org/10.1051/0004-6361/200913298>. arXiv: 0912.4166 [astro-ph.CO].
- Lusso, E., G. Worseck, J. F. Hennawi, J. X. Prochaska, C. Vignali, J. Stern, and J. M. O'Meara. 2015. The first ultraviolet quasar-stacked spectrum at  $z \approx 2.4$  from wfc3. *Monthly Notices of the Royal Astronomical Society* 449, no. 4 (April): 4204–4220. issn: 0035-8711. <https://doi.org/10.1093/mnras/stv516>. eprint: <https://academic.oup.com/mnras/article-pdf/449/4/4204/18753804/stv516.pdf>. <https://doi.org/10.1093/mnras/stv516>.
- Machacek, Marie E., Greg L. Bryan, and Tom Abel. 2001. Simulations of Pregalactic Structure Formation with Radiative Feedback. *ApJ* 548, no. 2 (February): 509–521. <https://doi.org/10.1086/319014>. arXiv: astro-ph/0007198 [astro-ph].
- Madau, Piero. 2018. Constraints on early star formation from the 21-cm global signal. *Monthly Notices of the Royal Astronomical Society* 480, no. 1 (October): L43–L47. <https://doi.org/10.1093/mnras/sly125>. arXiv: 1807.01316 [astro-ph.CO].
- Madau, Piero, and Tassos Fragos. 2017. Radiation Backgrounds at Cosmic Dawn: X-Rays from Compact Binaries. *The Astrophysical Journal* 840, no. 1 (May): 39. <https://doi.org/10.3847/1538-4357/aa6af9>. arXiv: 1606.07887 [astro-ph.GA].
- Madau, Piero, Emanuele Giallongo, Andrea Grazian, and Francesco Haardt. 2024. Cosmic Reionization in the JWST Era: Back to AGNs? *The Astrophysical Journal* 971, no. 1 (August): 75. <https://doi.org/10.3847/1538-4357/ad5ce8>. arXiv: 2406.18697 [astro-ph.CO].
- Madau, Piero, Avery Meiksin, and Martin J. Rees. 1997. 21 Centimeter Tomography of the Intergalactic Medium at High Redshift. *The Astrophysical Journal* 475, no. 2 (February): 429–444. <https://doi.org/10.1086/303549>. arXiv: astro-ph/9608010 [astro-ph].
- Maiolino, Roberto, Jan Scholtz, Emma Curtis-Lake, Stefano Carniani, William Baker, Anna de Graaff, Sandro Tacchella, et al. 2024. JADES: The diverse population of infant black holes at  $4 < z < 11$ : Merging, tiny, poor, but mighty. *A&A* 691 (November): A145. <https://doi.org/10.1051/0004-6361/202347640>. arXiv: 2308.01230 [astro-ph.GA].
- Marconi, A., G. Risaliti, R. Gilli, L. K. Hunt, R. Maiolino, and M. Salvati. 2004. Local supermassive black holes, relics of active galactic nuclei and the x-ray background. *Monthly Notices of the Royal Astronomical Society* 351, no. 1 (June): 169–185. issn: 0035-8711. <https://doi.org/10.1111/j.1365-2966.2004.07765.x>. <https://doi.org/10.1111/j.1365-2966.2004.07765.x>.
- Matteri, Antonio, Andrea Pallottini, and Andrea Ferrara. 2025. Can primordial black holes explain the overabundance of bright super-early galaxies? *arXiv e-prints* (March): arXiv:2503.01968. <https://doi.org/10.48550/arXiv.2503.01968>. arXiv: 2503.01968 [astro-ph.GA].
- Matthee, Jorryt, Rohan P. Naidu, Gabriel Brammer, John Chisholm, Anna-Christina Eilers, Andy Goulding, Jenny Greene, et al. 2024. Little Red Dots: An Abundant Population of Faint Active Galactic Nuclei at  $z \sim 5$  Revealed by the EIGER and FRESCO JWST Surveys. *ApJ* 963, no. 2 (March): 129. <https://doi.org/10.3847/1538-4357/ad2345>. arXiv: 2306.05448 [astro-ph.GA].
- Mazzolari, G., R. Gilli, M. Brusa, M. Mignoli, F. Vito, I. Prandoni, S. Marchesi, et al. 2024. Heavily obscured AGN detection: A radio versus X-ray challenge. *A&A* 687 (July): A120. <https://doi.org/10.1051/0004-6361/202348072>. arXiv: 2402.00109 [astro-ph.GA].
- McLeod, D J, C T Donnan, R J McLure, J S Dunlop, D Magee, R Begley, A C Carnall, et al. 2023. The galaxy UV luminosity function at  $z \approx 11$  from a suite of public JWST ERS, ERO, and Cycle-1 programs. *Monthly Notices of the Royal Astronomical Society* 527, no. 3 (November): 5004–5022. issn: 0035-8711. <https://doi.org/10.1093/mnras/stad3471>. eprint: <https://academic.oup.com/mnras/article-pdf/527/3/5004/54719193/stad3471.pdf>. <https://doi.org/10.1093/mnras/stad3471>.
- McQuinn, Matthew, and Ryan M. O'Leary. 2012. THE IMPACT OF THE SUPERSONIC BARYON-DARK MATTER VELOCITY DIFFERENCE ON THE  $z \sim 20$  21 cm BACKGROUND. *The Astrophysical Journal* 760, no. 1 (October): 3. <https://doi.org/10.1088/0004-637x/760/1/3>. <https://doi.org/10.1088/0004-637x/760/1/3>. <https://doi.org/10.1088/0004-637x/760/1/3>.
- McQuinn, Matthew, Oliver Zahn, Matias Zaldarriaga, Lars Hernquist, and Steven R. Furlanetto. 2006. Cosmological Parameter Estimation Using 21 cm Radiation from the Epoch of Reionization. *The Astrophysical Journal* 653, no. 2 (December): 815–834. <https://doi.org/10.1086/505167>. arXiv: astro-ph/0512263 [astro-ph].
- Meiksin, Avery, and Piero Madau. 2020. The impact of  $\text{Ly}\alpha$  emission line heating and cooling on the cosmic dawn 21-cm signal. *Monthly Notices of the Royal Astronomical Society* 501, no. 2 (December): 1920–1932. issn: 0035-8711. <https://doi.org/10.1093/mnras/staa3830>. eprint: <https://academic.oup.com/mnras/article-pdf/501/2/1920/35335652/staa3830.pdf>. <https://doi.org/10.1093/mnras/staa3830>.
- Mesinger, Andrei, and Steven Furlanetto. 2007. Efficient Simulations of Early Structure Formation and Reionization. *The Astrophysical Journal* 669, no. 2 (November): 663–675. <https://doi.org/10.1086/521806>. arXiv: 0704.0946 [astro-ph].

- Miralda-Escudé, Jordi. 2003. The Dark Age of the Universe. *Science* 300, no. 5627 (June): 1904–1909. <https://doi.org/10.1126/science.1085325>. arXiv: astro-ph/0307396 [astro-ph].
- Mirocha, Jordan, and Steven R. Furlanetto. 2019. What does the first highly redshifted 21-cm detection tell us about early galaxies? *Monthly Notices of the Royal Astronomical Society* 483, no. 2 (February): 1980–1992. <https://doi.org/10.1093/mnras/sty3260>. arXiv: 1803.03272 [astro-ph.GA].
- Mitchell-Wynne, Ketron, Asantha Cooray, Yongquan Xue, Bin Luo, William Brandt, and Anton Koekemoer. 2016. Cross-correlation between X-Ray and Optical/Near-infrared Background Intensity Fluctuations. *ApJ* 832, no. 2 (December): 104. <https://doi.org/10.3847/0004-637X/832/2/104>. arXiv: 1610.02015 [astro-ph.CO].
- Mittal, Shikhar, and Girish Kulkarni. 2022. Implications of the cosmological 21-cm absorption profile for high-redshift star formation and deep JWST surveys. *Monthly Notices of the Royal Astronomical Society* 515, no. 2 (September): 2901–2913. <https://doi.org/10.1093/mnras/stac1961>. arXiv: 2203.07733 [astro-ph.CO].
- Mittal, Shikhar, Anupam Ray, Girish Kulkarni, and Basudeb Dasgupta. 2022. Constraining primordial black holes as dark matter using the global 21-cm signal with X-ray heating and excess radio background. *Journal of Cosmology and Astroparticle Physics* 2022, no. 3 (March): 030. <https://doi.org/10.1088/1475-7516/2022/03/030>. arXiv: 2107.02190 [astro-ph.CO].
- Morey, Karna A., Anna-Christina Eilers, Frederick B. Davies, Joseph F. Hennawi, and Robert A. Simcoe. 2021. Estimating the Effective Lifetime of the  $z \sim 6$  Quasar Population from the Composite Proximity Zone Profile. *ApJ* 921, no. 1 (November): 88. <https://doi.org/10.3847/1538-4357/ac1c70>. arXiv: 2108.10907 [astro-ph.GA].
- Nabizadeh, Armin, Erik Zackrisson, Fabio Pacucci, Walter Peter Maksym, Weihui Li, Francesca Civano, Seth H. Cohen, et al. 2024. A search for high-redshift direct-collapse black hole candidates in the PEARLS north ecliptic pole field. *A&A* 683 (March): A58. <https://doi.org/10.1051/0004-6361/202347724>. arXiv: 2308.07260 [astro-ph.GA].
- Naidu, Rohan P., Pascal A. Oesch, Gabriel Brammer, Andrea Weibel, Yijia Li, Jorryt Matthee, John Chisholm, et al. 2025. A Cosmic Miracle: A Remarkably Luminous Galaxy at  $z_{\text{spec}} = 14.44$  Confirmed with JWST. *arXiv e-prints* (May): arXiv:2505.11263. <https://doi.org/10.48550/arXiv.2505.11263>. arXiv: 2505.11263 [astro-ph.GA].
- Natwariya, Pravin Kumar. 2021. Constraint on primordial magnetic fields in the light of ARCADE 2 and EDGES observations. *European Physical Journal C* 81, no. 5 (May): 394. <https://doi.org/10.1140/epjc/s10052-021-09155-z>. arXiv: 2007.09938 [astro-ph.CO].
- Nebrin, Olof, Sambit K. Giri, and Garrelt Mellema. 2023. Starbursts in low-mass haloes at Cosmic Dawn. I. The critical halo mass for star formation. *MNRAS* 524, no. 2 (September): 2290–2311. <https://doi.org/10.1093/mnras/stad1852>. arXiv: 2303.08024 [astro-ph.CO].
- Oesch, P. A., R. J. Bouwens, G. D. Illingworth, I. Labbé, and M. Stefanon. 2018. The Dearth of  $z \sim 10$  Galaxies in All HST Legacy Fields—The Rapid Evolution of the Galaxy Population in the First 500 Myr. *ApJ* 855, no. 2 (March): 105. <https://doi.org/10.3847/1538-4357/aab03f>. arXiv: 1710.11131 [astro-ph.GA].
- Ono, Yoshiaki, Yuichi Harikane, Masami Ouchi, Hidenobu Yajima, Makito Abe, Yuki Isobe, Takatoshi Shibuya, et al. 2023. Morphologies of Galaxies at  $z \gtrsim 9$  Uncovered by JWST/NIRCam Imaging: Cosmic Size Evolution and an Identification of an Extremely Compact Bright Galaxy at  $z \sim 12$ . *The Astrophysical Journal* 951, no. 1 (July): 72. <https://doi.org/10.3847/1538-4357/acd44a>. arXiv: 2208.13582 [astro-ph.GA].
- Pacucci, Fabio, and Abraham Loeb. 2024. The Redshift Evolution of the  $M_{\text{BH}} - M_{\text{star}}$  Relation for JWST's Supermassive Black Holes at  $z > 4$ . *ApJ* 964, no. 2 (April): 154. <https://doi.org/10.3847/1538-4357/ad3044>. arXiv: 2401.04159 [astro-ph.GA].
- Patil, Pallavi, Kristina Nyland, Mark Whittle, Carol Lonsdale, Mark Lacy, Colin Lonsdale, Dipanjan Mukherjee, et al. 2020. High-resolution VLA Imaging of Obscured Quasars: Young Radio Jets Caught in a Dense ISM. *ApJ* 896, no. 1 (June): 18. <https://doi.org/10.3847/1538-4357/ab9011>. arXiv: 2004.07914 [astro-ph.GA].
- Peca, Alessandro, Nico Cappelluti, C. Megan Urry, Stephanie LaMassa, Stefano Marchesi, Tonima Tasnim Ananna, Mislav Baloković, et al. 2023. On the Cosmic Evolution of AGN Obscuration and the X-Ray Luminosity Function: XMM-Newton and Chandra Spectral Analysis of the 31.3 deg<sup>2</sup> Stripe 82X. *ApJ* 943, no. 2 (February): 162. <https://doi.org/10.3847/1538-4357/acac28>. arXiv: 2210.08030 [astro-ph.GA].
- Pérez-González, Pablo G., Göran Östlin, Luca Costantin, Jens Melinder, Steven L. Finkelstein, Rachel S. Somerville, Marianna Annunziatella, et al. 2025. The rise of the galactic empire: luminosity functions at  $z \sim 17$  and  $z \sim 25$  estimated with the MIDIS+NGDEEP ultra-deep JWST/NIRCam dataset. *arXiv e-prints* (March): arXiv:2503.15594. <https://doi.org/10.48550/arXiv.2503.15594>. arXiv: 2503.15594 [astro-ph.GA].
- Planck Collaboration, N. Aghanim, Y. Akrami, M. Ashdown, J. Aumont, C. Baccigalupi, M. Ballardini, et al. 2020. Planck 2018 results. VI. Cosmological parameters. *Astronomy & Astrophysics* 641 (September): A6. <https://doi.org/10.1051/0004-6361/201833910>. arXiv: 1807.06209 [astro-ph.CO].
- Pober, J. C., B. J. Hazelton, A. P. Beardsley, N. A. Barry, Z. E. Martinot, I. S. Sullivan, M. F. Morales, et al. 2016. The Importance of Wide-field Foreground Removal for 21 cm Cosmology: A Demonstration with Early MWA Epoch of Reionization Observations. *The Astrophysical Journal* 819, no. 1 (March): 8. <https://doi.org/10.3847/0004-637X/819/1/8>. arXiv: 1601.06177 [astro-ph.IM].
- Pouliaxis, E., A. Ruiz, I. Georgantopoulos, F. Vito, R. Gilli, C. Vignali, Y. Ueda, et al. 2024. Active galactic nucleus X-ray luminosity function and absorption function in the Early Universe ( $3 \leq z \leq 6$ ). *A&A* 685 (May): A97. <https://doi.org/10.1051/0004-6361/202348479>. arXiv: 2401.13515 [astro-ph.GA].
- Pritchard, Jonathan R., and Abraham Loeb. 2008. Evolution of the 21cm signal throughout cosmic history. *Phys. Rev. D* 78, no. 10 (November): 103511. <https://doi.org/10.1103/PhysRevD.78.103511>. arXiv: 0802.2102 [astro-ph].
- Reis, Itamar, Anastasia Fialkov, and Rennan Barkana. 2020. High-redshift radio galaxies: a potential new source of 21-cm fluctuations. *Monthly Notices of the Royal Astronomical Society* 499, no. 4 (December): 5993–6008. <https://doi.org/10.1093/mnras/staa3091>. arXiv: 2008.04315 [astro-ph.CO].
- . 2021. The subtlety of Ly  $\alpha$  photons: changing the expected range of the 21-cm signal. *MNRAS* 506, no. 4 (October): 5479–5493. <https://doi.org/10.1093/mnras/stab2089>. arXiv: 2101.01777 [astro-ph.CO].
- Ripamonti, E., M. Mapelli, and S. Zaroubi. 2008. Radiation from early black holes – I. Effects on the neutral intergalactic medium. *Monthly Notices of the Royal Astronomical Society* 387, no. 1 (June): 158–172. <https://doi.org/10.1111/j.1365-2966.2008.13104.x>. arXiv: 0802.1857 [astro-ph].
- Sacchi, Andrea, and Akos Bogdan. 2025. Chandra Rules Out Super-Eddington Accretion For Little Red Dots. *arXiv e-prints* (May): arXiv:2505.09669. <https://doi.org/10.48550/arXiv.2505.09669>. arXiv: 2505.09669 [astro-ph.GA].
- Satyavolu, Sindhu, Girish Kulkarni, Laura C. Keating, and Martin G. Haehnelt. 2023. The need for obscured supermassive black hole growth to explain quasar proximity zones in the epoch of reionization. *MNRAS* 521, no. 2 (May): 3108–3126. <https://doi.org/10.1093/mnras/stad729>. arXiv: 2209.08103 [astro-ph.GA].
- Shaver, P. A., R. A. Windhorst, P. Madau, and A. G. de Bruyn. 1999. Can the reionization epoch be detected as a global signature in the cosmic background? *Astronomy & Astrophysics* 345 (May): 380–390. <https://doi.org/10.48550/arXiv.astro-ph/9901320>. arXiv: astro-ph/9901320 [astro-ph].



- Shen, Xuejiao, Mark Vogelsberger, Michael Boylan-Bolton, Sandro Tacchella, and Rohan P. Naidu. 2024. Early galaxies and early dark energy: a unified solution to the hubble tension and puzzles of massive bright galaxies revealed by JWST. *Monthly Notices of the Royal Astronomical Society* 533, no. 4 (October): 3923–3936. <https://doi.org/10.1093/mnras/stae1932>. arXiv: 2406.15548 [astro-ph.GA].
- Sheth, Ravi K., and Giuseppe Tormen. 1999. Large-scale bias and the peak background split. *Monthly Notices of the Royal Astronomical Society* 308, no. 1 (September): 119–126. <https://doi.org/10.1046/j.1365-8711.1999.02692.x>. arXiv: astro-ph/9901122 [astro-ph].
- Sicilia, Alex, Andrea Lapi, Lumen Boco, Francesco Shankar, David M. Alexander, Viola Allevato, Carolin Villforth, et al. 2022. The Black Hole Mass Function across Cosmic Time. II. Heavy Seeds and (Super)Massive Black Holes. *ApJ* 934, no. 1 (July): 66. <https://doi.org/10.3847/1538-4357/ac7873>. arXiv: 2206.07357 [astro-ph.GA].
- Sims, Peter H., and Jonathan C. Pober. 2020. Testing for calibration systematics in the EDGES low-band data using Bayesian model selection. *MNRAS* 492, no. 1 (February): 22–38. <https://doi.org/10.1093/mnras/stz3388>. arXiv: 1910.03165 [astro-ph.CO].
- Singh, Saurabh, Nambissan T. Jishnu, Ravi Subrahmanyan, N. Udaya Shankar, B. S. Girish, A. Raghunathan, R. Somashekar, K. S. Srivani, and Mayuri Sathyanarayana Rao. 2022. On the detection of a cosmic dawn signal in the radio background. *Nature Astronomy* 6 (February): 607–617. <https://doi.org/10.1038/s41550-022-01610-5>. arXiv: 2112.06778 [astro-ph.CO].
- Singh, Saurabh, Ravi Subrahmanyan, N. Udaya Shankar, Mayuri Sathyanarayana Rao, Anastasia Fialkov, Aviad Cohen, Rennan Barkana, et al. 2018. SARAS 2 Constraints on Global 21 cm Signals from the Epoch of Reionization. *The Astrophysical Journal* 858, no. 1 (May): 54. <https://doi.org/10.3847/1538-4357/aabae1>. arXiv: 1711.11281 [astro-ph.CO].
- Smith, Brent M., Rogier A. Windhorst, Seth H. Cohen, Anton M. Koekemoer, Rolf A. Jansen, Cameron White, Sanchayeeta Borthakur, et al. 2020. The Lyman Continuum Escape Fraction of Galaxies and AGN in the GOODS Fields. *The Astrophysical Journal* 897, no. 1 (July): 41. <https://doi.org/10.3847/1538-4357/ab8811>. arXiv: 2004.04360 [astro-ph.GA].
- Spinoglio, Luigi, Juan Antonio Fernández-Ontiveros, and Matthew A. Malkan. 2024. The Spectral Energy Distributions and Bolometric Luminosities of Local AGN: Study of the Complete 12  $\mu$ m AGN Sample. *ApJ* 964, no. 2 (April): 117. <https://doi.org/10.3847/1538-4357/ad23e4>. arXiv: 2312.13661 [astro-ph.GA].
- Sun, Yang, George H. Rieke, Jianwei Lyu, Meredith A. Stone, Zhiyuan Ji, Pierluigi Rinaldi, Christopher N. A. Willmer, and Yongda Zhu. 2025. The  $M_{\star} - M_{\text{BH}}$  Relation Evolution from  $z \sim 6$  to the Present Epoch. *arXiv e-prints* (March): arXiv:2503.03675. <https://doi.org/10.48550/arXiv.2503.03675>. arXiv: 2503.03675 [astro-ph.GA].
- Telfer, Randal C., Wei Zheng, Gerard A. Kriss, and Arthur F. Davidsen. 2002. The Rest-Frame Extreme-Ultraviolet Spectral Properties of Quasi-stellar Objects. *ApJ* 565, no. 2 (February): 773–785. <https://doi.org/10.1086/324689>. arXiv: astro-ph/0109531 [astro-ph].
- Tompkins, Scott A., Simon P. Driver, Aaron S. G. Robotham, Rogier A. Windhorst, Claudia del P. Lagos, T. Vernstrom, and Andrew M. Hopkins. 2023. The cosmic radio background from 150 MHz to 8.4 GHz and its division into AGN and star-forming galaxy flux. *MNRAS* 521, no. 1 (May): 332–353. <https://doi.org/10.1093/mnras/stad116>. arXiv: 2301.03699 [astro-ph.GA].
- Treu, T., G. Roberts-Borsani, M. Bradac, G. Brammer, A. Fontana, A. Henry, C. Mason, et al. 2022. The GLASS-JWST Early Release Science Program. I. Survey Design and Release Plans. *ApJ* 935, no. 2 (August): 110. <https://doi.org/10.3847/1538-4357/ac8158>. arXiv: 2206.07978 [astro-ph.GA].
- Valdés, M., A. Ferrara, M. Mapelli, and E. Ripamonti. 2007. Constraining dark matter through 21-cm observations. *Monthly Notices of the Royal Astronomical Society* 377, no. 1 (May): 245–252. <https://doi.org/10.1111/j.1365-2966.2007.11594.x>. arXiv: astro-ph/0701301 [astro-ph].
- Vanden Berk, Daniel E., Gordon T. Richards, Amanda Bauer, Michael A. Strauss, Donald P. Schneider, Timothy M. Heckman, Donald G. York, et al. 2001. Composite Quasar Spectra from the Sloan Digital Sky Survey. *AJ* 122, no. 2 (August): 549–564. <https://doi.org/10.1086/321167>. arXiv: astro-ph/0105231 [astro-ph].
- Venditti, Alessandra, Julian B. Munoz, Volker Bromm, Seiji Fujimoto, Steven L. Finkelstein, and John Chisholm. 2025. Bursty or heavy? The surprise of bright Population III systems in the Reionization era. *arXiv e-prints* (May): arXiv:2505.20263. <https://doi.org/10.48550/arXiv.2505.20263>. arXiv: 2505.20263 [astro-ph.GA].
- Vijarnwannaluk, Bovornpratch, Masayuki Akiyama, Malte Schramm, Yoshihiro Ueda, Yoshiaki Matsuoka, Yoshiaki Toba, Marcin Sawicki, Stephen Gwyn, and Janek Pflugrad. 2022. The Obscured Fraction of Quasars at Cosmic Noon. *ApJ* 941, no. 1 (December): 97. <https://doi.org/10.3847/1538-4357/ac9c07>. arXiv: 2209.07797 [astro-ph.GA].
- Visbal, Eli, Greg L. Bryan, and Zoltán Haiman. 2020. Self-consistent semi-analytic modeling of feedback during primordial star formation and reionization. *The Astrophysical Journal* 897, no. 1 (July): 95. <https://doi.org/10.3847/1538-4357/ab994e>. <https://doi.org/10.3847/2F1538-4357%2F6ab994e>.
- Wang, Yijun, Tao Wang, Luis C. Ho, Yuxing Zhong, and Bin Luo. 2024. The fundamental plane of black hole activity for low-luminosity radio active galactic nuclei across  $0 < z < 4$ . *A&A* 689 (September): A327. <https://doi.org/10.1051/0004-6361/202449732>. arXiv: 2402.17991 [astro-ph.GA].
- Whitler, Lily, Daniel P. Stark, Michael W. Topping, Brant Robertson, Marcia Rieke, Kevin N. Hainline, Ryan Endsley, et al. 2025. The *zrsim9* galaxy UV luminosity function from the JWST Advanced Deep Extragalactic Survey: insights into early galaxy evolution and reionization. *arXiv e-prints* (January): arXiv:2501.00984. <https://doi.org/10.48550/arXiv.2501.00984>. arXiv: 2501.00984 [astro-ph.GA].
- Windhorst, Rogier A., F. X. Timmes, J. Stuart B. Wyithe, Mehmet Alpaslan, Stephen K. Andrews, Daniel Coe, Jose M. Diego, et al. 2018. On the Observability of Individual Population III Stars and Their Stellar-mass Black Hole Accretion Disks through Cluster Caustic Transits. *ApJS* 234, no. 2 (February): 41. <https://doi.org/10.3847/1538-4365/aaa760>. arXiv: 1801.03584 [astro-ph.GA].
- Witstok, Joris, Peter Jakobsen, Roberto Maiolino, Jakob M. Helton, Benjamin D. Johnson, Brant E. Robertson, Sandro Tacchella, et al. 2025. Witnessing the onset of reionization through Lyman- $\alpha$  emission at redshift 13. *Nature* 639, no. 8056 (March): 897–901. <https://doi.org/10.1038/s41586-025-08779-5>. arXiv: 2408.16608 [astro-ph.GA].
- Woods, Tyrone E., Bhaskar Agarwal, Volker Bromm, Andrew Bunker, Ke-Jung Chen, Sunmyon Chon, Andrea Ferrara, et al. 2019. Titans of the early Universe: The Prato statement on the origin of the first supermassive black holes. *Publications of the Astronomical Society of Australia* 36 (August): e027. <https://doi.org/10.1017/pasa.2019.14>. arXiv: 1810.12310 [astro-ph.GA].
- Wouthuysen, S. A. 1952. On the excitation mechanism of the 21-cm (radio-frequency) interstellar hydrogen emission line. *AJ* 57 (January): 31–32. <https://doi.org/10.1086/106661>.

- Yang, G., K. I. Caputi, C. Papovich, P. Arrabal Haro, M. B. Bagley, P. Behroozi, E. F. Bell, et al. 2023. CEERS Key Paper. VI. JWST/MIRI Uncovers a Large Population of Obscured AGN at High Redshifts. *ApJ* 950, no. 1 (June): L5. <https://doi.org/10.3847/2041-8213/acd639>. arXiv: 2303.11736 [astro-ph.GA].
- Yang, Jinyi, Feige Wang, Xiaohui Fan, Joseph F. Hennawi, Frederick B. Davies, Minghao Yue, Eduardo Banados, et al. 2020. Pōniuā'ena: A Luminous  $z = 7.5$  Quasar Hosting a 1.5 Billion Solar Mass Black Hole. *The Astrophysical Journal* 897, no. 1 (July): L14. <https://doi.org/10.3847/2041-8213/ab9c26>. arXiv: 2006.13452 [astro-ph.GA].
- Yung, L. Y. Aaron, Rachel S. Somerville, and Kartheik G. Iyer. 2025.  $\Lambda$ CDM is still not broken: empirical constraints on the star formation efficiency at  $z \sim 12 - 30$ . *arXiv e-prints* (April): arXiv:2504.18618. <https://doi.org/10.48550/arXiv.2504.18618>. arXiv: 2504.18618 [astro-ph.GA].